Monthly Notices
of the
ROYAL ASTRONOMICAL SOCIETY

Mon. Not. R. Astron. Soc. **416,** 3138–3159 (2011) doi:10.1111/j.1365-2966.2011.19262.x

SN 2009jf: a slow-evolving stripped-envelope core-collapse supernova⋆

S. Valenti,[1,2]† M. Fraser,[1] S. Benetti,[2] G. Pignata,[3,4] J. Sollerman,[5] C. Inserra,[6,7] E. Cappellaro,[2] A. Pastorello,[1] S. J. Smartt,[1] M. Ergon,[5] M. T. Botticella,[2] J. Brimacombe,[8] F. Bufano,[2] M. Crockett,[9] I. Eder,[10] D. Fugazza,[11] J. B Haislip,[12] M. Hamuy,[4] A. Harutyunyan,[13] K. M. Ivarsen,[12] E. Kankare,[14,15] R. Kotak,[1] A. P. LaCluyze,[12] L. Magill,[1] S. Mattila,[5,14] J. Maza,[4] P. A. Mazzali,[2,16] D. E. Reichart,[12] S. Taubenberger,[16] M. Turatto[17] and L. Zampieri[2]

[1]*Astrophysics Research Centre, School of Mathematics and Physics, Queen's University Belfast, Belfast BT7 1NN*
[2]*INAF Osservatorio Astronomico di Padova, Vicolo dell'Osservatorio 5, 35122 Padova, Italy*
[3]*Departamento de Ciencias Fisicas, Universidad Andres Bello, Avda. Republica 252 Santiago, Chile*
[4]*Departamento de Astronomia, Universidad de Chile, Casilla 36-D Santiago, Chile*
[5]*The Oskar Klein Centre, Department of Astronomy, Stockholm University, AlbaNova, 10691 Stockholm, Sweden*
[6]*INAF Osservatorio Astrofisico di Catania, Via S. Sofia 78, 95123 Catania, Italy*
[7]*Dipartimento di Fisica ed Astronomia, Universitá di Catania, Sezione Astrofisica, Via S.Sofia 78, 95123 Catania, Italy*
[8]*Coral Towers Observatory, Coral Towers, Esplanade, Cairns 4870, Australia*
[9]*Department of Physics, University of Oxford, Keble Road, Oxford OX1 3RH*
[10]*Medve u. 15, H-1027 Budapest, Hungary*
[11]*INAF-Osservatorio Astronomico di Brera, via Bianchi 46, 23807 Merate, Italy*
[12]*University of North Carolina at Chapel Hill, Campus Box 3255, Chapel Hill, NC 27599-3255, USA*
[13]*Fundación Galileo Galilei-INAF, Telescopio Nazionale Galileo, 38700 Santa Cruz de la Palma, Tenerife, Spain*
[14]*Tuorla Observatory, Department of Physics & Astronomy, University of Turku, Väisäläntie 20, FI-21500 Piikkiö, Finland*
[15]*Nordic Optical Telescope, Apartado 474, E-38700 Santa Cruz de La Palma, Spain*
[16]*Max-Planck-Institut für Astrophysik, Karl-Schwarzschild-Str. 1, 85741 Garching bei München, Germany*
[17]*INAF Osservatorio Astronomico di Trieste, Via Tiepolo 11, 34143 Trieste, Italy*

Accepted 2011 June 15. Received 2011 June 15; in original form 2011 May 12

ABSTRACT

We present an extensive set of photometric and spectroscopic data for SN 2009jf, a nearby Type Ib supernova (SN), spanning from ∼20 d before *B*-band maximum to 1 yr after maximum. We show that SN 2009jf is a slowly evolving and energetic stripped-envelope SN and is likely from a massive progenitor (25–30 $M_\odot$). The large progenitor's mass allows us to explain the complete hydrogen plus helium stripping without invoking the presence of a binary companion. The SN occurred close to a young cluster, in a crowded environment with ongoing star formation. The spectroscopic similarity with the He-poor Type Ic SN 2007gr suggests a common progenitor for some SNe Ib and Ic. The nebular spectra of SN 2009jf are consistent with an asymmetric explosion, with an off-centre dense core. We also find evidence that He-rich Ib SNe have a rise time longer than other stripped-envelope SNe, however confirmation of this result and further observations are needed.

Key words: supernovae: general – supernovae: individual: SN 2009jf – galaxies: individual: NGC 7479.

1 INTRODUCTION

Type Ib supernovae (SNe) are observationally defined by the absence of hydrogen (H) and presence of helium (He) in their spectra at early phases. They are thought to come from massive stars ($M \geq 8\,M_\odot$) which have lost their H envelope, but retained part of their He envelope before exploding. SNe Ic show neither H nor He features in their early spectra, and arise from massive stars which have also lost most of their He envelope. A group of SNe that show H features at early phases, but do not follow the typical light curve seen for the H-rich Type II SNe, and instead evolve photometrically and spectroscopically into SNe Ib are known as Type IIb SNe. These are also thought to come from massive star progenitors which have lost most (but not all) of their H envelope before exploding.

⋆This paper is based on observations with several telescopes, including NTT(184.D-1151), VLT-UT1(085.D-0750,386.D-0126), NOT, WHT, TNG, PROMPT, Ekar, Calar Alto and Liverpool Telescope.

†E-mail: stefano.valenti@oapd.inaf.it

SNe IIb, Ib and Ic are often collectively termed 'stripped-envelope SNe' (Clocchiatti & Wheeler 1997).

We emphasize that the apparent lack of H and/or He lines in an early spectrum does not preclude the presence of these elements in the ejecta. Branch et al. (2002) analysed a large sample of SN Ib spectra, and suggested that H is often present also in SNe Ib, though this element is very difficult to detect after maximum. They also found that He is often present outside the photosphere (detached), in particular at late phases. Similar studies of SNe Ic (Branch et al. 2006; Elmhamdi et al. 2006) suggest that traces of H and He may be also present in some SNe Ic. The presence of He and/or H in some stripped-envelope SNe could be an indication that the progenitor has been stripped continuously (which can leave thin layers of H or He on the progenitor) as opposed to strong episodic mass loss, which would likely completely strip the progenitor. Furthermore, the small observational differences between He rich (Ib) and He poor (Ic) SNe may suggest a similar origin, with progenitors of SNe Ic simply being more strongly stripped than those of SNe Ib.

An important open issue on SNe Ib/c is whether they come from relatively high-mass Wolf–Rayet (WR) stars ($M > 20$–$25\,M_{\odot}$) that have been stripped of H and part of their He envelope by radiatively driven winds, or from lower mass progenitors ($M > 11\,M_{\odot}$) which have been stripped of their envelope by a binary companion (Podsiadlowski, Joss & Hsu 1992).

Several statistical studies have been performed on the environments of stripped-envelope SNe in order to characterize the Ib and Ic progenitor populations. Many have focused on metallicity as a key parameter driving mass loss in single stars and hence determining the relative numbers of Types II, Ib and Ic SNe. Metallicity is also important in binary models (Eldridge, Izzard & Tout 2008), and influences the number of WR stars produced as well as the predicted ratios of Ibc SN. Rotation rates are also thought to be dependent on initial stellar metallicity (Georgy et al. 2009). Initial studies of the global properties of host galaxies suggested that the number of SNe Ic relative to the number of SNe Ib increases with metallicity (Prieto, Stanek & Beacom 2008; Anderson & James 2009; Boissier & Prantzos 2009). However, more recent measurements of the nebular oxygen abundances at the sites of SNe Ib and Ic now suggest there is little difference between the samples (Anderson et al. 2010; Leloudas et al. 2011; Modjaz et al. 2011). From these results, there is no unambiguous evidence that Ibc SNe are produced in more metal-rich regions than type II SNe, or that Ib and Ic SNe originate in different metallicity regimes.

The relatively high frequency of SNe Ib/c (30 per cent of all core-collapse SNe by volume) and the lack of progenitor detections (Crockett 2009; Smartt 2009) support the idea that at least some of the SNe Ib/c progenitors are massive stars in binary systems (Podsiadlowski et al. 1992; Fryer et al. 2007; Eldridge et al. 2008). On the other hand, the extreme kinetic energies inferred for some stripped-envelope SNe, namely those associated with gamma-ray bursts (GRBs), are indicative of a high-mass progenitor which does not need necessary binarity to lose its envelope.

Excluding the extreme cases, for most stripped-envelope SNe discriminating between the progenitor scenarios is more tricky. In principle, one may argue that SNe which eject more material probably come from more massive stars, while SNe with low-mass ejecta may come from less massive progenitors in binary systems. On the other hand, if fall-back occurs (where a portion of the SN ejecta falls back on to the newly born compact remnant at the centre) even very massive stars may eject only a small amount of material. A detailed analysis of the elemental abundances in the ejecta is then a useful diagnostic. For example, oxygen and carbon are expected to be more abundant in ejecta of a SN from a massive progenitor, due to the larger progenitor core mass. However, from an observational point of view, the number of stripped-envelope SNe with detailed ejecta characterization is still small. Recent discoveries have also pointed out the largely unexplored diversity in He-rich SNe, for example the wide range of ejected mass and energy as typified by SN 2007Y (Stritzinger et al. 2009) and SN 2008D (Mazzali et al. 2008), respectively, or the case of SN 1999dn, for years considered a prototype of SNe Ib, but recently proposed to be a highly energetic SN from a massive progenitor (Benetti et al. 2011).

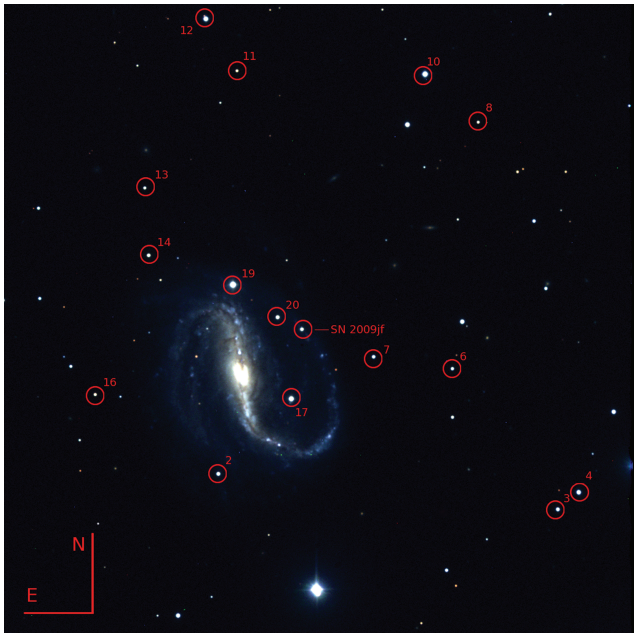

Figure 1. The field of view ($9 \times 9\,\mathrm{arcmin}^2$) of SN 2009jf. This *R*-band Calar Alto image (2009 November 18) was taken 34 days after the *B*-band maximum. The local sequence stars have been numbered to calibrate the photometry (magnitudes reported in Tables C1 and C2).

In this framework, every new nearby SN Ib discovered represents an opportunity to increase our understanding of these events. SN 2009jf, a nearby SN which was discovered early after the explosion, is a perfect target to enlarge the sample of well-studied SNe Ib.

In this paper we present the full set of data we collected for SN 2009jf, from the ultraviolet (UV) to optical and near-infrared (NIR). The structure of the paper is as follows. In Section 2 we describe the set of data collected and its calibration. In Section 3 we present the photometric data, and in Sections 4 and 5 the optical and NIR spectra of SN 2009jf. In Section 6, we discuss the properties of the host galaxy NGC 7479 (see Fig. 1) and provide an analysis of the progenitor using archival pre-explosion data. In Section 7, we discuss the main physical parameters of the progenitor of SN 2009jf at the moment of the explosion through an analysis of the bolometric light curve. In the final section, we summarize our results and discuss our conclusions. We note that Sahu et al. (2011) have also presented a spectrophotometric study of SN 2009jf in the optical with which we will compare our results with.

2 DISCOVERY AND FOLLOW-UP

SN 2009jf was discovered (Li, Cenko & Filippenko 2009) on 2009 September 27.33 (UT dates are used throughout this paper) with the Katzman Automatic Imaging Telescope (KAIT) during the Lick

Observatory Supernova Search (Filippenko et al. 2001). The SN is located at coordinates $\alpha = 23^{h}04^{m}52\overset{s}{.}98$ and $\delta = +12^{\circ}19'59\overset{''}{.}5$ (equinox J2000), which is $53\overset{''}{.}8$ W and $36\overset{''}{.}5$ N of the centre of the host galaxy NGC 7479. The host is a barred spiral galaxy, with an intriguing jet-like radio continuum feature. The alignment of this jet, which is in the opposite orientation to the optical arms, has been suggested to be consistent with NGC 7479 having recently undergone a minor merger (Laine & Beck 2008). SN 2009jf was not visible in a KAIT unfiltered image taken 4 days before discovery (September 23.32) (>19.2 mag; Li et al. 2009) and was classified on September 29.1 as a young Type Ib SN similar to SN 1999ex (Kasliwal et al. 2009; Sahu, Anupama & Gurugubelli 2009). Itagaki, Kaneda & Yamaoka (2009) reported the detection of a source close to the position of the SN in several images obtained over the past few decades. A rough estimate of the absolute magnitude of the source in the pre-discovery images (−14.5 mag) led Itagaki et al. (2009) to initially suggest a luminous blue variable as the progenitor of SN 2009jf. However, we have undertaken a more thorough analysis of the archival images, and the source is more likely a cluster close to the position where the SN occurred (see Section 6). SN 1990U, which was a SN Type Ic, also exploded in this galaxy (Filippenko, Shields & Richmond 1990; Pennypacker, Perlmutter & Marvin 1990).

Being discovered well before maximum, and in a nearby host galaxy, SN 2009jf was targeted for an intensive spectrophotometric follow-up campaign by the European Large Programme (ELP) SN Collaboration,[1] together with the Millennium Center for Supernova Science (MCSS).

Our photometric and spectroscopic monitoring campaign for SN 2009jf began on 2009 October 1, just 7 days after explosion (see Section 3). We observed the SN every ∼2–3 d in Sloan and Bessel filters, with slightly more relaxed coverage (one observation every ∼4–5 d) in the NIR bands. From the beginning of December, ∼2.5 months after explosion, the SN was no longer visible from the Southern hemisphere. From then on, it was observed from the Northern hemisphere with a more relaxed cadence (one observation every week) until it disappeared behind the sun at ∼105 d after explosion. The SN was recovered as soon as it was visible again in 2010 June with observations that extended until October to cover the nebular phase.

We used several of the facilities available to the ELP collaboration, and also the five PROMPT[2] (Reichart et al. 2005) telescopes used by the MCSS project. The *Swift* telescope also observed SN 2009jf at UV wavelengths, and the publicly available data from this have been included in our analysis. However, due to the strong contamination from the close-by cluster, the *Swift* $uvm2$ and $uvw2$ filter data are not usable (see Appendix A) and thus not reported.

NGC 7479 is one of the most beautiful nearby face-on galaxies, and a popular target for amateur astronomers. Some of the images obtained by amateurs have been useful in constraining the explosion epoch, and these have been added to our data set. In particular, we obtained images of NGC 7479 taken on September 23, 24, 26 and 27, providing excellent coverage close to the explosion epoch.[3]

[1] http://graspa.oapd.inaf.it/index.php?option=com_content&view=article&id=68&Itemid=93

[2] Panchromatic Robotic Optical Monitoring and Polarimetry Telescopes.

[3] http://eder.csillagaszat.hu/deepsky/350D/sn2009jf/ sn2009jf_eder_en.htm

The *UBVRI* data ranging from ∼1 to ∼380 d after explosion are reported in Table C3, while the *ugriz* data are reported in Table C4. All data calibrated to the Landolt system are in the Vega system, while the data calibrated to Sloan are in the AB system (Smith et al. 2002).

Spectroscopic monitoring started on 2009 October 1, 7 days after explosion, and continued during the photospheric phase until the beginning of the seasonal gap at ∼105 d after explosion. More spectra were collected in the nebular phase, when the SN became visible again. In total, we collected 20 optical and four IR spectra of SN 2009jf (see Section 4). Details of our data reduction methods are reported in Appendix A.

2.1 Archival observations

To search for a progenitor in pre-explosion data (see Smartt 2009, for a review), we queried all suitable publicly available image archives of which we are aware of.

The most useful images for constraining the pre-explosion environment and progenitor of SN 2009jf are from the Wide-Field Planetary Camera 2 (WFPC2) on-board the *Hubble Space Telescope* (*HST*). The site of SN 2009jf was observed for a total of 2000 s in the $F569W$ filter and 1800 s in the $F814W$ filter on 1995 October 16.

Pre-explosion data were also available from many ground-based observatories, but these images, which have a typical seeing of 1 arcsec, are not of sufficient quality to resolve the complex region where the SN exploded (see Section 6.2). The same is true for the *Spitzer* IRAC and *XMM–Newton* OM images.

However, several of these deep pre-explosion ground-based images were used as templates for application of the template-subtraction technique for our photometry (see Appendix A). In particular, we used the following images: U, B and I images from William Herschel Telescope (WHT) (1990 August 17, 17 and 18, respectively), a V-band image from the European Southern Observatory (ESO) New Technology Telescope (NTT) (1992 December 2) and an R-band image from the Nordic Optical Telescope (NOT) (2009 September 13).

To identify a potential progenitor in *HST* data, we obtained deep images of SN 2009jf and its environs on 2009 October 24 and 25 with the ESO Very Large Telescope (VLT), and Nasmyth Adaptive Optics System and Near-Infrared Imager and Spectrograph (NaCo). We used the K_S filter with the S54 camera.[4] A late-time observation was obtained on 2010 September 16, but the SN had faded in the NIR to the point where it was not significantly brighter than the nearby cluster, and so these data were of no use in locating the progenitor.

3 PHOTOMETRY

To constrain the explosion epoch, we used the pre-discovery images of NGC 7479 taken by I. Eder on September 23–27. The first observation on September 23 was before the first non-detection of SN 2009jf at the KAIT telescope (Li et al. 2009). Using these images taken on September 23 as a template, we performed image subtraction on the images taken over the following days (24, 26 and 27) with the same telescope. The SN is marginally detected in B, V and R bands on September 26, while nothing is detected in the same bands on September 24 (see Fig. 2). The detections

[4] Pixel scale of 0.054 arcsec over a 56 × 56 arcsec^2 field of view.

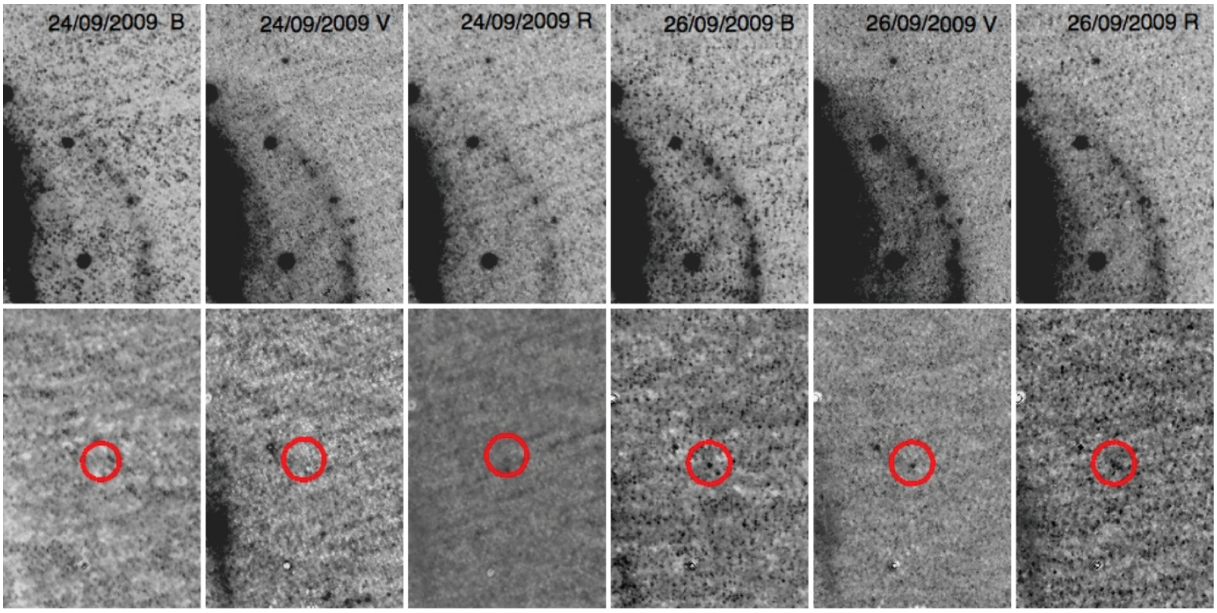

Figure 2. *BVR* images of SN 2009jf obtained on 2009 September 24 and 26 (upper panels) together with difference images obtained by subtracting images in the same filters obtained on 2009 September 23 (lower panels). The marginal detections on September 26 and the non-detections on September 24 constrain the explosion epoch to 2009 September 25 (JD = 245 5099.5) ±1 which is one of the best constrained explosion epochs for a stripped-envelope SN. North is up and east to the left.

on September 26 and the non-detections on September 24, making the reasonable assumption that the object was rapidly brightening before maximum, constrain the explosion epoch to September 25 (JD = 245 5099.5) ±1 d, which is one of the best constrained explosion epochs for a stripped-envelope SN (not associated with a GRB).

All the collected photometric data are shown in Fig. 3. The data of Sahu et al. (2011) are also overplotted for comparison.

As shown in Fig. 3, our photometry is consistent with that of Sahu et al. (2011) at early phases, but at later epochs their photometry appears to systematically overestimate the SN flux as compared to our template-subtraction photometry (see Appendix A). SN 2009jf is a clear case where proper template subtraction has to be used to avoid the contamination from the bright background. There is also a shift between our *U*-band photometry and that of Sahu et al. (2011), with our photometry being fainter by ∼0.2 mag. At late phases, the differences are even larger, again probably due to the overestimation of the SN magnitude when using point spread function (PSF)-fitting techniques as opposed to template-subtraction photometry.

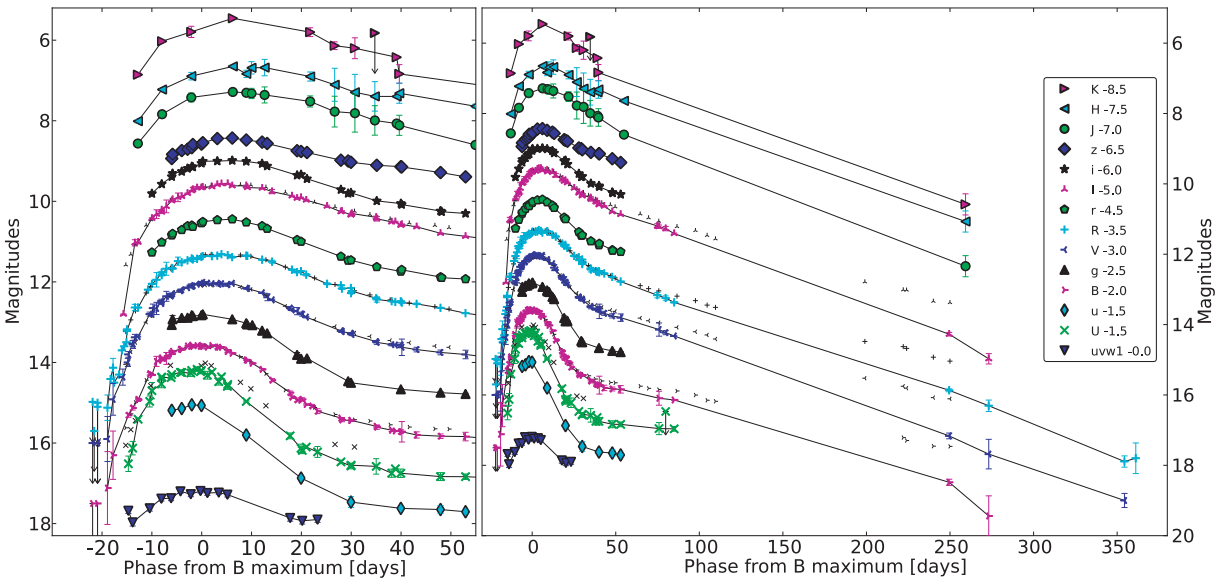

Figure 3. The light curves of SN 2009jf in the *uvw*1 − *UuBgVrRiIzJHK* bands. In the left-hand panel, we show the data from explosion to two months after *B* maximum (JD = 245 5119.4 ± 1.0; 2009 October 14). In the right-hand panel, we show the full light curves in all bands. The data of Sahu et al. (2011) are overplotted with smaller symbols for comparison.

Table 1. Main parameters for light curves of SN 2009jf. The *UBVRI* magnitudes are in the Vega system, the *ugriz* magnitudes in the AB system.

Parameter	*U*	*B*	*V*	*R*	*I*
Date of max (JD −240 0000)	55117. ± 2.0	55119.4 ± 1.0	55121.5 ± 1.0	55124.0 ± 1.0	55124.7 ± 1.0
Apparent magnitude at max	15.70 ± 0.05	15.56 ± 0.02	15.03 ± 0.01	14.83 ± 0.01	14.59 ± 0.01
Absolute magnitude at max	−17.73 ± 0.26	−17.75 ± 0.22	−18.12 ± 0.18	−18.24 ± 0.15	−18.37 ± 0.14
Late-time decline γ (mag d^{-1})	–	0.0088 ± 0.0014	0.0136 ± 0.0007	0.0161 ± 0.0002	0.0171 ± 0.0011
Phase range	–	55–105	63–105	60–105	58–105
Parameter	*u*	*g*	*r*	*i*	*z*
Date of max (JD −240 0000)	55 117. ± 2.0	55 120.6 ± 1.0	55 123.7 ± 1.0	55 125.0 ± 1.0	55 125.5 ± 1.0
Apparent magnitude at max	16.56 ± 0.04	15.29 ± 0.01	14.96 ± 0.02	14.97 ± 0.02	14.95 ± 0.03
Absolute magnitude at max	−16.88 ± 0.26	−17.97 ± 0.21	−18.13 ± 0.17	−18.02 ± 0.14	−17.94 ± 0.12
Late-time decline γ (mag d^{-1})	–	0.015 ± 0.002	0.020 ± 0.003	0.021 ± 0.002	0.016 ± 0.001
Phase range	–	49–73	55–73	55–73	48–73

SN 2009jf reached its maximum luminosity on 2009 October 14 at 15.56 ± 0.02 mag in the *B* band. It peaked 2.4 d earlier in the *U* band, and 2.1, 4.6 and 5.3 d later in the *V*, *R* and *I* bands, respectively (Table 1). The rise times to maximum were ∼17.5, 19.9, 22.0, 24.5 and 25.2 d respectively in the *UBVRI* bands. This is one of the slowest rise times ever observed for a classical SN Ib/c. Using a distance modulus of 32.65 ± 0.1 mag and a galactic reddening of $E(B-V) = 0.112$ mag (Schlegel, Finkbeiner & Davis 1998) and internal $E(B-V) = 0.05$ mag (see Section 6), SN 2009jf reached a maximum absolute magnitude in the *R* band of −18.24 mag, brighter than SNe 2008D (−17.26 mag; Mazzali et al. 2008) and 1999ex (−17.78 mag; Stritzinger et al. 2002) and comparable with the massive Type Ic core-collapse SN 2004aw (−18.22 mag; Taubenberger et al. 2006). After maximum the light curves of SN 2009jf are not very different from those of other SNe Ib/c, although with a slower than normally observed decline both soon after maximum and after the inflection point at ∼30 d past maximum. The resulting light curve peak for SN 2009jf is broad, suggesting a massive ejecta and/or a small expansion velocity which keeps the ejecta optically thick for a long time.

The late-time luminosity decline rates were computed via weighted linear least-squares fits to the observations and are reported in Table 1 together with other key parameters measured from the light curves. The late-time slopes are in all bands steeper than those expected if the energy source is ^{56}Co → ^{56}Fe decay with complete trapping of the γ-rays [0.98 mag (100 d)$^{-1}$] – as is normally observed in stripped-envelope core-collapse SNe.

The colour evolution of SN 2009jf (see Fig. 4) resembles that of other stripped-envelope SNe. The SN becomes redder with time as the ejecta expand and the temperature decreases. The $B-V$ colour is 0.3 mag at +15 d from explosion and reaches a maximum ∼+40 d after explosion ($B-V \sim 1$ mag). In the first two weeks after explosion, some stripped-envelope SNe display a bluer $B-V$ colour ($B-V \sim 0$ mag) (e.g. SNe 1993J, 2008D). Other stripped-envelope SNe (e.g. SNe 1999ex, 2008ax) are blue immediately after explosion, show a $B-V$ colour ∼0.5–1 mag at one week and then become blue again ($B-V \sim 0.3$ mag) at two weeks after explosion. SN 2009jf shows a behaviour similar to this second group of objects, but less extreme with $B-V \sim 0$ mag in the first two photometric points, $B-V \sim 0.5$ mag at one week and $B-V \sim 0.3$ mag two weeks from explosion. The blue colour of some SNe in the first days after explosion has been interpreted as an evidence for shock break-out (Stritzinger et al. 2002; Chevalier & Soderberg 2010).

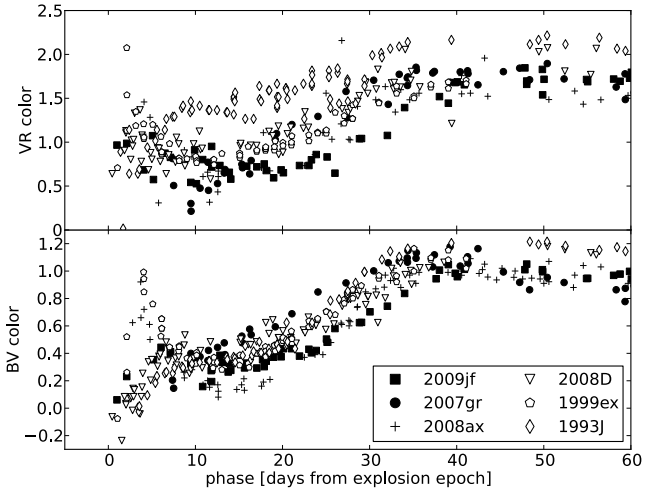

Figure 4. The $B-V$ and $V-R$ colour curves for a sample of stripped-envelope core-collapse SNe.

With the caveat of the large uncertainty in these first measurements, this may also be the case for SN 2009jf.

4 PHOTOSPHERIC SPECTRA

A subset of the optical photospheric spectra of SN 2009jf is shown in Fig. 5, the instrumental configurations used at each epoch are listed in Table 2, while details of data reduction are in Appendix A. The four NIR spectra are shown in Fig. 6 together with spectra of other stripped-envelope SNe. The first spectrum of SN 2009jf was observed 13 d before maximum (one week after explosion). At early phases, SN 2009jf shows a blue continuum with the typical features of a stripped-envelope SN already visible, namely Fe II λλ4924, 5018, 5169, Ca II λλ8498, 8542, 8662, Ca II λλ3934, 3968 and O I λ7770. The lines are partially blended, but not as much as for broad-lined Ic (BLIc) SNe or the energetic Ib SN 2008D (Mazzali et al. 2008).

With time, the temperature decreases, the spectra of SN 2009jf become redder and lines which form deeper in the ejecta (at lower velocity) become more prominent. The identification of the features at ∼5800 and ∼6200 Å is more complicated as these regions are usually densely populated with lines from several different elements such as Na, He, H, Si, C and Ne.

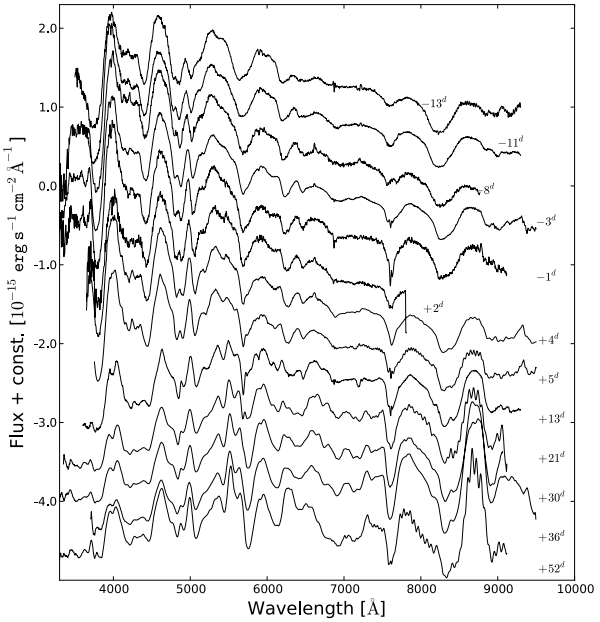

Figure 5. A subset of the collected photospheric spectra of SN 2009jf. The spectra are in the observer frame.

The possible presence of H and He is very important to understand the progenitor star evolution. In more massive progenitor ($M >$ 25–30 $M_\odot$), the ratio between He (or H) and the other elements of the ejecta should be smaller than in less massive progenitors ($11\,M_\odot < M < 25\,M_\odot$). This will be discussed in the following section.

4.1 He identification

The He lines, with the exception of the He I line at 2.058 μm, are in spectral regions which are densely populated by other features. The identification of He lines is further complicated by the fact that they often form in non-local thermodynamic equilibrium conditions, giving uncertain line-strength ratios (Lucy 1991).

For some recent detailed studies of SNe Ib/c, the detection or non-detection of the He I line at 2.058 μm was the clearest way to distinguish SNe Ib from SNe Ic (Hamuy et al. 2002; Valenti et al. 2008b; Modjaz et al. 2009; Stritzinger et al. 2009). For SN 2009jf, He I at 2.058 μm is clearly detected in our NIR spectra at 6, 39 and 52 d after maximum and marginally detected also at 10 d before *B*-band maximum (see Fig. 6). Thus He is definitely present in SN 2009jf, confirming the SN classification as a SN Ib. However, while for most SNe Ib the He lines increase in intensity from the explosion until two weeks after maximum, in SN 2009jf the He lines are weaker than in other SNe Ib, with the lines at λλ6678, 7065 almost disappearing two weeks after *B*-band maximum. In Fig. 7, we show the spectral regions where He lines should be visible. The He I λλ5876, 6678 are clearly seen in Fig. 7 (minimum of the narrow P-Cygni absorption is indicated with a dashed line). On the red side of the He line at λ5876, a broader absorption becomes more intense over time. This feature was identified by Sahu et al. (2011) as He at much lower velocity than at early phases. However, no sign of such absorption is visible for the He lines at λλ6678, 7065

Table 2. Journal of spectroscopic observations.

Date	JD 240 0000	Phase[a] (d)	Range (Å)	Resolution FWHM[b] (Å)	Equipment[c]
2009 Oct 02	55106.62	−13	3200–10100	10	TNG+DOLORES+LRB/LRR
2009 Oct 04	55108.63	−11	3600–9300	10	VLT+FORS2+300V/300I
2009 Oct 06	55111.40	−8	3200–8750	10	CA+CAFOSC+b200
2009 Oct 07	55112.37	−7	6150–10100	10	CA+CAFOCS+r200
2009 Oct 12	55116.57	−3	3200–10100	10	TNG+DOLORES+LRB/LRR
2009 Oct 13	55118.46	−1	3200–9200	15	NOT+ALFOSC+gr4
2009 Oct 16	55121.48	+2	3550–7750	23	A1.82+AFOSC+gr4
2009 Oct 18	55123.42	+4	3550–10000	23/35	A1.82+AFOSC+gr4/gr2
2009 Oct 19	55124.61	+5	3400–9650	14	NTT+EFOSC+gr11/16
2009 Oct 27	55132.60	+13	3600–9300	10	VLT+FORS2+300V/300I
2009 Nov 04	55140.39	+21	3200–9200	15	NOT+ALFOSC+gr4
2009 Nov 13	55149.39	+30	3200–9200	17	NOT+ALFOSC+gr4
2009 Nov 19	55155.35	+36	3800–10000	12	CA+CAFOCS+g200
2009 Dec 05	55171.34	+52	3200–9200	15	NOT+ALFOSC+gr4
2009 Dec 27	55193.35	+74	3800–10000	12	CA+CAFOCS+g200
2010 Jan 07	55149.39	+85	3200–9200	15	NOT+ALFOSC+gr4
2010 Jun 19	55366.88	+247	3200–9200	18	NTT+EFOSC+gr11/16
2010 Jul 08	55385.66	+266	3200–9200	3	WHT+ISIS+R300B/R316R
2010 Oct 04	55473.57	+354	3600–9200	25	NTT+EFOSC+gr13
2010 Oct 11	55480.51	+361	3600–9300	10	VLT+FORS2+300V/300I
2009 Oct 04	55109.51	−10	8700–24700	18/35	TNG+NICS+IJ/HK
2009 Oct 21	55125.58	+6	9400–24000	23/33	NTT+SOFI+GB/GR
2009 Nov 23	55158.58	+39	8700–24700	18/36	TNG+NICS+IJ/HK
2009 Dec 05	55171.36	+52	9300–24700	23/33	NTT+SOFI+GB/GR

[a]Relative to *B*-band maximum light (JD = 245 5119.4).
[b]Full width at half-maximum (FWHM) of night-sky emission lines.
[c]A1.82 = Asiago Ekar 1.82-m telescope; NOT = Nordic Optical Telescope; TNG = Telescopio Nazionale Galileo; NTT = ESO New Technology Telescope; CA = Calar Alto 2.2-m Telescope; WHT = William Herschel Telescope; VLT =ESO Very Large Telescope.

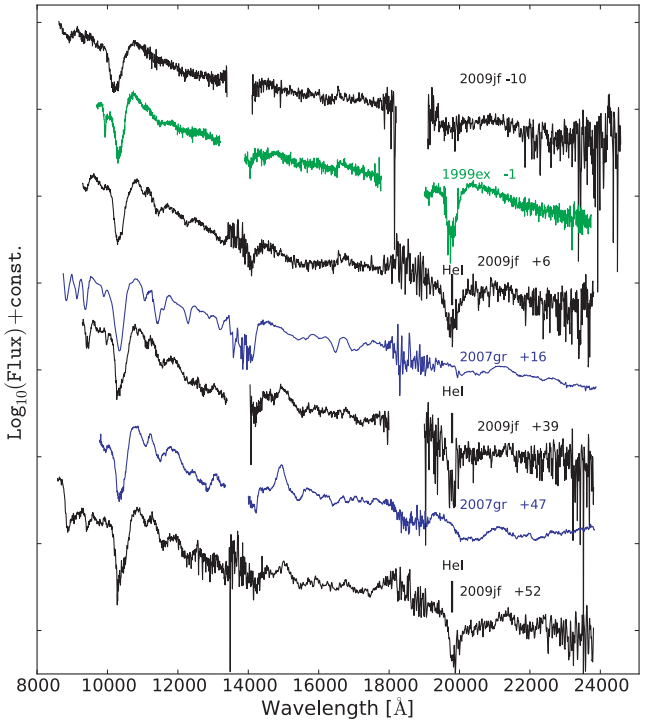

Figure 6. The IR spectra of SN 2009jf are shown at the SN rest wavelength together with those of SN 2007gr (Ic) and SN 1999ex (Ib). He I λ2.058 μm is marked in the spectra of SN 2009jf.

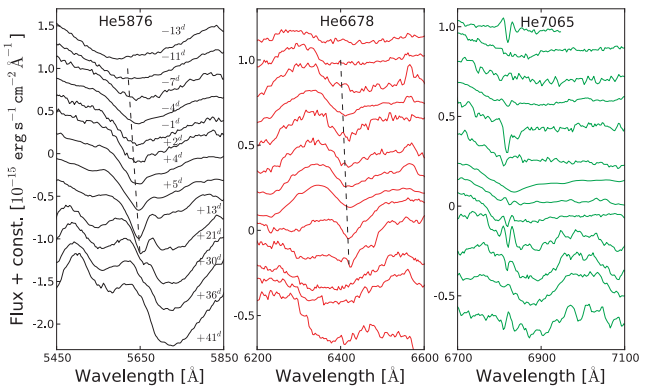

Figure 7. The spectral regions where the He lines (at λλ5876, 6678 and 7065) should be visible (spectra at rest frame). The absorption at ∼5700 Å visible at late phases is unlikely to be He, as suggested by Sahu et al. (2011) since all other He lines at that velocity are missing both in the optical and in the NIR.

and 2.058 μm. In order to better constrain the presence of He, we used the SYNOW[5] spectrum synthesis code to model two spectra of SN 2009jf.

4.1.1 −11 d from B-band maximum

We have modelled the merged optical (VLT+FORS2) and NIR (TNG+NICS) spectra taken −11 and −10 d before *B*-band maximum, respectively. The spectrum was reproduced including lines from Fe II, O I, Ca II, Mg II, Sc II, Ti II, Si II, Ne I and He I (upper

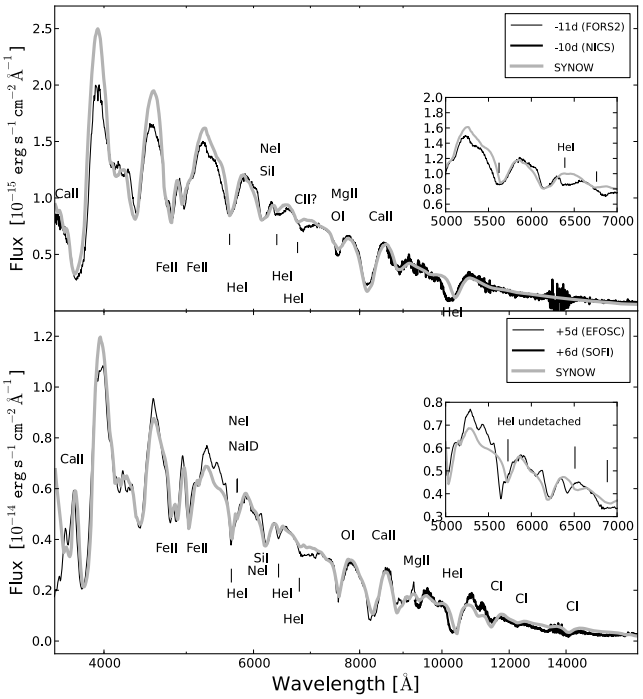

Figure 8. SYNOW fit of the spectra of SN 2009jf at −11 and +6 d from *B*-band maximum light. Before maximum, the He lines are present in the SYNOW fit, while in the inset, using Na instead of He, the line at ∼6500 Å, which is likely He I λ6678 is not reproduced. After maximum most of the line at 5700 Å is reproduced by Na I D. Only undetached lines of He are identified. The inset shows a SYNOW spectrum with undetached He. The spectra are at rest frame.

panel, Fig. 8). We used a photospheric velocity of 13 500 km s^{-1} and line optical depths that vary as e^{-v/v_e} with $v_e = 2000$ km s^{-1}. The features at 6100 Å were well reproduced by a combination of Si II and Ne I, while He I (undetached)[6] is able to reproduce both the feature at ∼5600 Å and the one at ∼6500 Å. The presence of C II cannot be ruled out, but while C II λ7235 would improve the fit of the absorption at ∼7000 Å, the C II λ6580 line would deteriorate the fit at ∼6400 Å. At this epoch, the He I at 2.058 μm is not visible in the NIR spectrum (see Fig. 6). For this reason, we also considered the possibility that the absorption at ∼5600 Å is Na I D instead of He I. However, with Na, instead of He, the fit will also fail to reproduce the features at ∼6500 Å, which is likely He I (λ6678) (see inset in upper panel in Fig. 8). Helium is also visible at 2.058 μm (see Fig. 6), though not very strong. We note that early NIR spectra are also available for another SN Ib (SN 2008D), in which the He I at 2.058 μm is also marginally visible at high velocity also at early phases (Modjaz et al. 2009). We hence consider the He identification quite robust.

4.1.2 +5 d from B-band maximum

The NTT+EFOSC (+5 d) and NTT+SOFI (+6 d) spectra and SYNOW fit are shown in the lower panel of Fig. 8. We used the same ions as for the pre-maximum spectrum, plus Na I and C I at a velocity of 8200 km s^{-1}. C I is needed to fit some of the features between 10 000 and 16 000 Å, while Na I D is needed to reproduce part of the spectrum at ∼5600 Å. He I is mainly responsible for the

[5] http://www.nhn.ou.edu/∼parrent/synow.html

[6] Lines that form at the photospheric velocity.

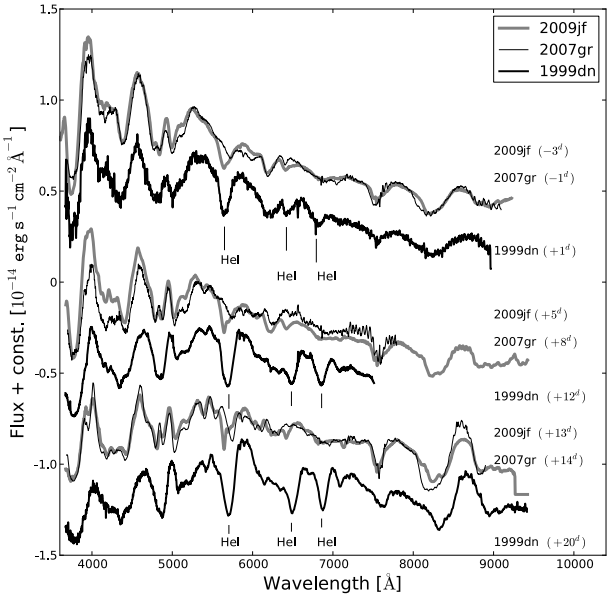

Figure 9. Three spectra of SN 2009jf are compared with those of SNe 2007gr and 1999dn. At all epochs the spectra of SN 2009jf are almost identical to those of SN 2007gr, with the sole exception of the He lines. SN 1999dn shows strong He absorption features, in contrast to both SNe 2009jf and 2007gr. All spectra are at rest frame.

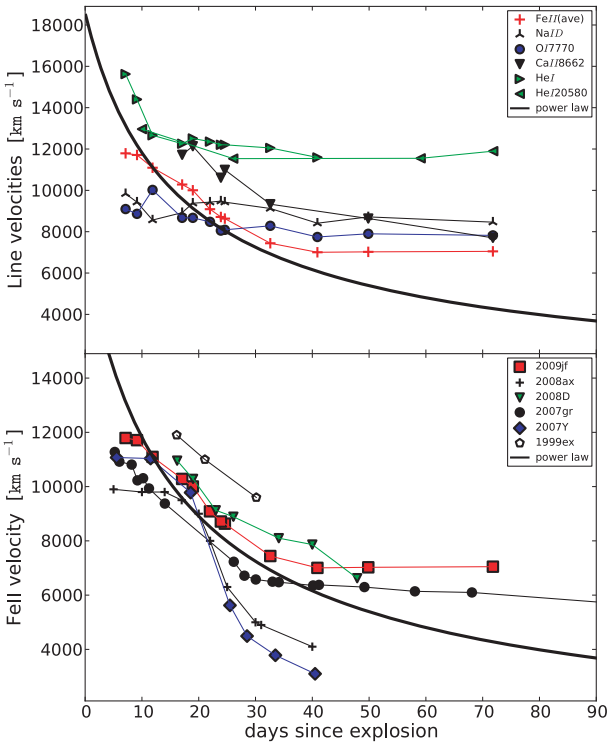

Figure 10. Upper panel: line velocities of SN 2009jf. The Na I D and He I minima have been measured by simultaneously fitting two Gaussians to the absorption feature at ∼5600 Å. Lower panel: the photospheric velocity evolution of SN 2009jf in comparison with those of a set of stripped-envelope SNe. All velocities were measured in IRAF with a Gaussian fit to the minimum of the line. In the both panel, the solid curves show the power-law fit to the photospheric velocities of a sample of SNe Ib from Branch et al. (2002).

blue narrow component of this feature with a detached velocity of 12 000 km s^{-1}. The detached He is also responsible for the line at ∼6500 Å. We investigated the possible presence of undetached He I, but in this case the He velocity is too low to reproduce correctly the absorption at ∼6500 Å (see lower inset panel in Fig. 8). Also, as we will see in the next section, the photospheric velocity at which the He I feature at 2.058 μm forms (measured from the minima of the P-Cygni absorption) is consistent with detached He. The photospheric velocity of He I at 2.058 μm remains constant from +6 to +52 d after *B*-band maximum.

Summarizing the optical and IR spectral analysis, we can conclude that the layer where the He lines form is located at a velocity between 12 000 and 16 000 km s^{-1}. It appears undetached at early phases, but becomes detached at 1–2 weeks after maximum. This is not surprising, as similar behaviour has already been observed in other SNe Ib (Branch et al. 2002). Regarding the presence of H, while a small amount cannot be completely ruled out, in both spectra there is no clear improvement in the fit when H is included. Moreover, there is no evidence (as observed for some SNe Ib) of Hβ features in the early spectrum. Hence SN 2009jf is likely a H-poor stripped-envelope SN, with a relatively small amount of He (mainly detached). This is confirmed by comparing the spectra of SN 2009jf with other SNe Ib/c (see Fig. 9). Across a range of phases, SN 2009jf is almost identical to the He-poor SN 2007gr (Valenti et al. 2008a; Hunter et al. 2009), with differences only in the region of the most prominent He features. For comparison, some spectra of the Ib SN 1999dn (Benetti et al. 2011) are shown with more prominent He features. Apart from the Ib classification, we could also regard SN 2009jf as a SN Ic that exploded with a small amount of He left in a high-velocity shell at 12 000–16 000 km s^{-1}.

4.2 Photospheric velocity

In the previous section, we claimed the presence of a detached layer of He at ∼12 000 km s^{-1}. This is also evident in Fig. 10 (upper panel), where the velocity evolution for different ions is plotted. The isolated He I line at ∼2 μm confirms the presence of detached He, while there is no sign in the IR spectra of He at low velocity.

Different lines form in different regions of the ejecta, in part due to the differing physical conditions (temperature and density), but also due to the stratification of elements within the ejecta. The Ca II lines form in the outer parts of the photosphere (as can be seen from their higher velocities), while O and Fe lines form in the inner part. The Fe II lines usually provide a good estimate of the photospheric velocity. Comparing with other stripped-envelope SNe, SN 2009jf has quite a high photospheric velocity, slightly lower than SNe 1999ex and 2008D but higher than SNe 2007Y and 2008ax. In particular, at late phases (70 d after explosion), SN 2009jf still has an optically thick photosphere at 7000 km s^{-1}. The evolution of the photospheric velocity of SN 2009jf resembles that of SN 2007gr, but with velocities which are ∼1000 km s^{-1} greater at almost all epochs. The similarity in the spectra (see previous section) and in the photospheric velocity evolution suggests that SN 2009jf had a progenitor similar to that of SN 2007gr, albeit slightly more massive and with more He left at the time of the explosion.

5 NEBULAR SPECTRA

After SN 2009jf became visible again in June 2010, we obtained spectra at 247, 266, 354 and 361 d after *B*-band maximum (see Fig. 11). At these late epochs the SN ejecta are optically thin, allowing us to observe the innermost parts of the ejecta where lines

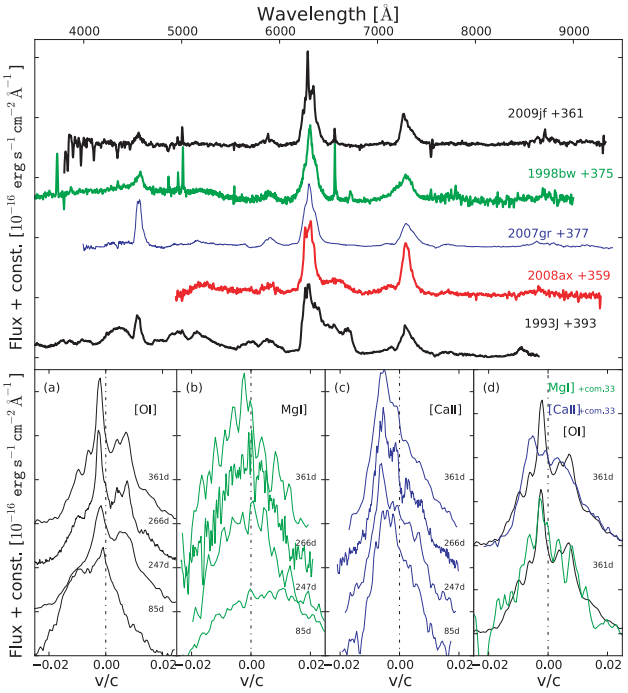

Figure 11. Upper panel: nebular spectra (at rest frame) of a sample of stripped-envelope SNe at 1 year from *B*-band maximum. Bottom panel: evolution of the main nebular features visible in the nebular spectra of SN 2009jf: (a) [O I], (b) Mg I] and (c) [Ca II]. In panel (d) we show at 361 d after *B*-band maximum, the comparison between the [O I] profile and profiles of the [Ca II] and Mg I] modified with a second component to reproduce the [O I] doublet (see text).

are mainly in emission. Several studies have been performed on nebular spectra of stripped-envelope SNe to investigate the geometry of the explosion (Mazzali et al. 2005; Maeda et al. 2008; Modjaz et al. 2008b; Taubenberger et al. 2009) as the nebular lines approximately represent a one-dimensional line-of-sight projection of the three-dimensional distribution of elements.

The most prominent emission lines are the [O I] λλ6300, 6364 doublet, Mg I] λ4571 and [Ca II] λλ7291, 7323. Several features of Fe II are also visible (but highly blended) from 4500 to 5500 Å. These are prominent only in the brightest stripped-envelope SNe (e.g. in SN 1998bw; Mazzali et al. 2001). The [O I] doublet is best suited to probe the explosion geometry, as the [Ca II] feature can be partially contaminated by [O II] λλ7320, 7330, and the Mg I] line is less intense and contaminated by Fe lines (at ∼100 d after explosion). Oxygen has also the advantage that it is the most abundant element in strongly stripped core-collapse SNe. A drawback is that it is a doublet with a line ratio sensitive to the temperature and density where the lines form.

It has been predicted and observed that the ratio of the oxygen lines λ6300/λ6364 increases with time from a ratio of 1:1 to a ratio of 3:1 in H-rich SNe (Leibundgut et al. 1991; Spyromilio & Pinto 1991; Chugai 1992). For stripped-envelope SNe, Taubenberger et al. (2009) suggested that the conditions during the nebular phase in the oxygen layer always give a ratio of 3:1. Milisavljevic et al. (2010), on the other hand, suggested that the [O I] line ratio may be close to 1:1 in several of these SNe, in order to explain the fact that SNe Ib show a double peak for the O feature more often than SNe Ic (without invoking a highly asymmetric explosion). Recently, Hunter et al. (2009) and Taubenberger et al. (2011) demonstrated that for SN 2007gr and SN 2008ax magnesium and oxygen had a similar distribution within the ejecta if the ratio of the oxygen lines at λ6300/λ6364 was fixed at 3:1. This similar distribution is expected from nucleosynthesis models (Maeda et al. 2006). Furthermore, Maurer et al. (2010) suggested that the apparent double peak at the position of the oxygen doublet is due to a high-velocity Hα absorption which, when superimposed on the oxygen lines, gives the appearance of a double peak. All SNe in the sample analysed by Maurer et al. (2010) are SNe IIb.

SN 2009jf also shows an oxygen feature with a complex structure that resembles a double peak profile. But since SN 2009jf does not show H features either at early or nebular phases, we consider unlikely that the [O I] profile of SN 2009jf is due to contamination from high-velocity H. This is also supported by the comparisons with Mg I] at λ4571 and [Ca II] at λλ7291, 7323 on day +361; if we take into account the doublet nature of the [O I] and artificially add a second component (redshifted and scaled to 1/3 of the flux) to the Mg I] and [Ca II] lines,[7] then the profiles of [O I], modified-Mg I] and modified-[Ca II] all have similar profiles as shown in the bottom panel (d) of Fig. 11. The similar profiles suggest that mixing is important in the progenitor of SN 2009jf since oxygen, magnesium and calcium have similar distributions within the ejecta, and that the oxygen profile is not due to Hα contamination.

If we assume that the mass of an element at a particular velocity is simply proportional to the emitted flux at that same velocity, the O profile (as those of Mg and Ca) is consistent with an asymmetric explosion, with a large part of the material ejected away from the observer. Sahu et al. (2011) also discussed the nature of the oxygen profile, and suggested large-scale clumping or a unipolar jet as the explanation. Here we propose an alternative geometry, which reproduces the oxygen profile with four different components (see upper panel of Fig. 12) coming from different parts of the ejecta. Taking into account that the [O I] line is a doublet (two lines separated by 64 Å and with a ratio ∼3:1), there are two clear narrow lines at 6285 and 6349 Å in the oxygen profile that may be interpreted as an off-centre dense core that is blueshifted by ∼700 km s^{-1}. The ratio of these two lines seems slightly lower than 3:1, suggesting a high density in this blob. Blueward and redward by ∼50 Å with respect to the off-centre dense core, we identify further blobs[8] of oxygen-rich material that may be interpreted as clumps. In this scenario, the rest of the oxygen (the broader component of the O line) is uniformly distributed in the ejecta[9]. A schematic reconstruction of the geometry is shown in Fig. 12 (lower panel). Within our simplifying assumption of mass proportional to flux, the dense off-centre core would contain ∼20 per cent of the oxygen mass, the clumps ∼10 per cent, while the rest of the oxygen mass would be distributed uniformly. We performed this analysis on the spectra at both +266 and +361 d after *B*-band maximum, obtaining similar results, as there is no significant evolution in the nebular spectra over this time period.

A caveat on the above discussion should be added. While the assumption that the oxygen mass distribution is proportional to the oxygen lines flux is reasonable, the random directions of material ejection in asymmetric explosions should produce stripped-envelope SNe with observables (e.g. line profiles) isotropically distributed. Inspecting the sample of nebular spectra of Taubenberger

[7] As the [Ca II] feature is a close doublet, it has been considered here as a single line.

[8] The two components of the blobs have ratios of ∼3:1.

[9] This is reproduced with two Gaussians (ratio ∼3:1) close to zero velocity.

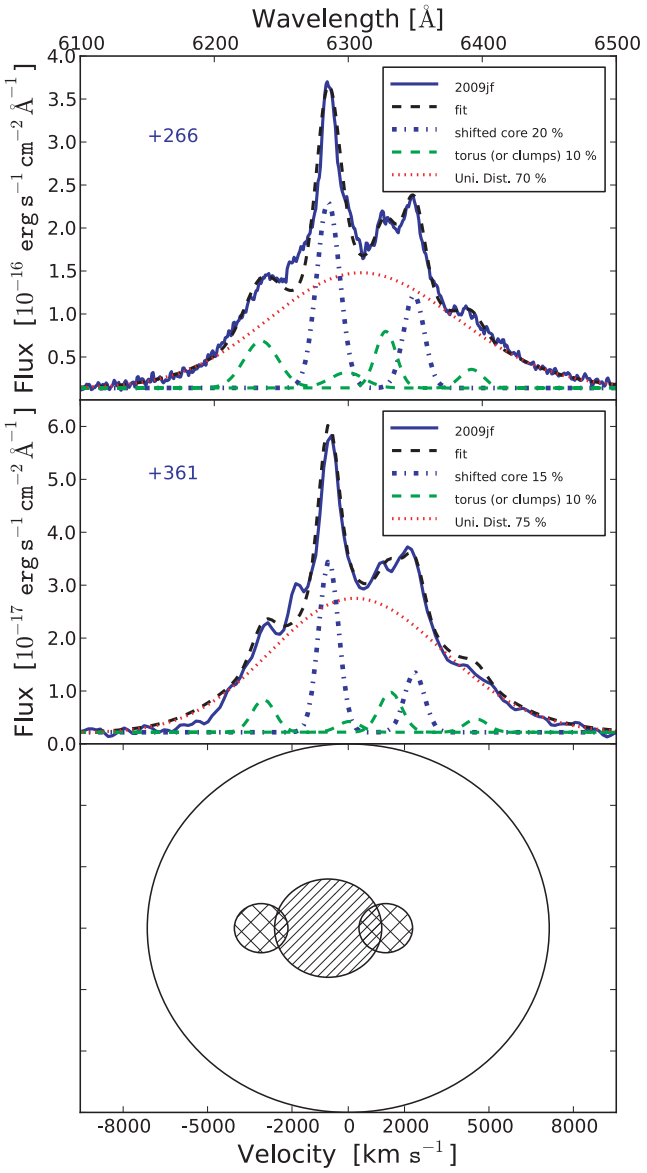

Figure 12. Oxygen line profile of SN 2009jf at +266 and +361 d from *B* maximum (upper and middle panels). If we assume that the oxygen line flux to trace the oxygen mass, SN 2009jf could be an asymmetric explosion, with an off-axis core (∼20 per cent of the oxygen flux/mass) surrounded by clumps. The remaining oxygen (∼70 per cent) is distributed uniformly throughout the ejecta. In the lower panel, a schematic reconstruction of the geometry is shown.

et al. (2009) (and including some recent discoveries), a number of SNe have been found showing blueshifted, off-centre line cores, while SNe with redshifted off-centre line cores have not been detected so far. This investigation is complicated by the fact that the oxygen profile may show blueshifted line peaks also at early phases (<200 d, when the ejecta are not fully transparent) or at very late phases due to dust formation. However, the amount of blueshift of the oxygen line peaks in the above mentioned spectra do not show any time evolution, leading us to rule out the dust formation or still opaque ejecta as likely explanations. Nevertheless, the lack of detections of SN spectra with redshifted oxygen profiles is puzzling, and an obvious explanation cannot be provided.

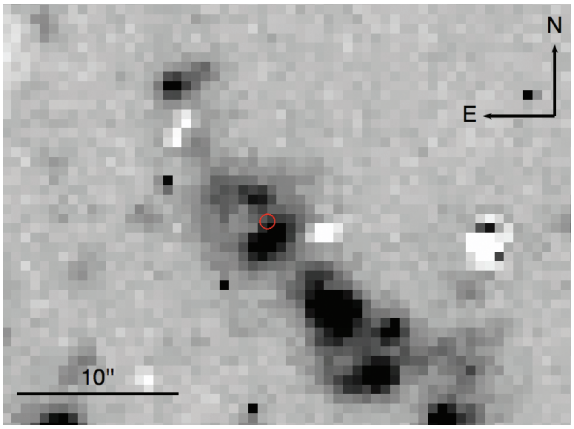

Figure 13. Continuum-subtracted Hα image of NGC7479 with the SN position indicated with a circle. The radius of the circle is 10 times the uncertainty in transformation used to determine the SN position.

6 HOST-GALAXY PROPERTIES

The host galaxy of SN 2009jf, NGC 7479, is a face-on spiral galaxy in the Pegasus constellation. It is relatively nearby (μ = 32.65 mag)[10] and quite asymmetric, with strong star formation along most of the luminous western arm (Laine & Gottesman 1998). SN 2009jf occurred in this arm, at the location of an extended star-forming region (see Fig. 13). NGC 7479 also displays some intriguing properties at radio wavelengths, with a radio continuum in the reverse direction to the optical arms (Laine & Beck 2005), which has been suggested to be the result of a minor merger.

The early spectra and the colour evolution of SN 2009jf are quite blue, suggesting that the light from SN 2009jf is absorbed and reddened by a relatively small amount of interstellar dust both in the Milky Way and in the host galaxy NGC 7479. While the Milky Way component is easily removed using maps of the Galactic dust distribution and a standard extinction law [$E(B-V) = 0.112$ mag; Schlegel et al. 1998], evaluating the extinction in NGC 7479 is more difficult. In principle, assuming an average dust-to-gas ratio, the reddening can be estimated by measuring the gas column density of interstellar lines from Na I D absorption. It is common practice to derive the host-galaxy extinction from its relation with the equivalent width (EW) of the Na I D line. Mostly using a sample of SNe Ia for which the reddening has been calculated using the Lira relation (Phillips et al. 1999), Turatto, Benetti & Cappellaro (2003) found that SNe appear to split on two slopes that give quite different EW(NaID) versus reddening relations. For SN 2009jf, we used the early spectra with high signal-to-noise ratio in order to separate the contribution to the Na I D absorption of the Milky Way from that of host system. Two small Na I D absorptions are visible in several spectra at 5893 Å (Galactic) and at 5941 Å (host system) (see Fig. 14). The EW measured for each absorption slightly changes among the spectra (0.4–0.9 Å for the Galactic absorption and 0.2–0.4 Å for the one in the host system). This is probably due to the different signal-to-noise ratios in the spectra, the spectral resolution and/or contamination from other lines. On the other hand, the ratio of the two absorptions is almost constant, with the Galactic one being twice as strong as that in the host system. Assuming a similar dust-to-gas ratio in NGC 7479 and in the Milky Way and the Galactic reddening in the direction of SN 2009jf reported by Schlegel

[10] Using a radial velocity corrected for in-fall on to Virgo of 2443 km s^{-1} and a Hubble constant of 72 km s^{-1} Mpc^{-1}.

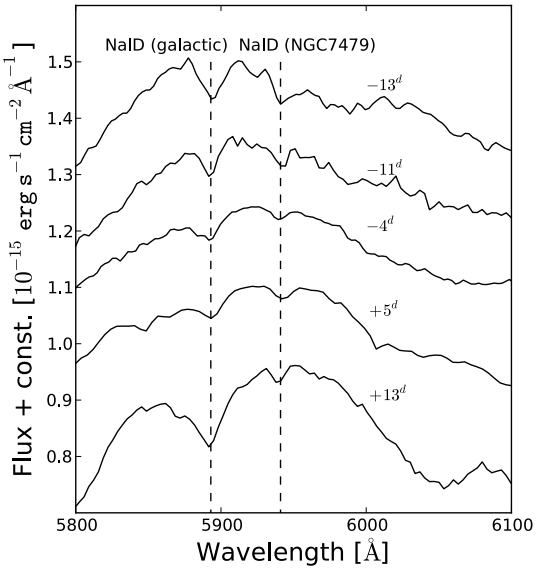

Figure 14. Low-resolution spectra of SN 2009jf in the region of the Galactic and host-galaxy Na I D absorptions.

et al. (1998), we obtain an $E(B-V)_{7479} \sim 0.05$ mag. Due to the uncertainty of the method and the fact that the EW measurement is uncertain, we adopt a host-galaxy reddening of $E(B-V)_{7479} = 0.05 \pm 0.05$ mag. The main parameters for NGC 7479 are reported in Table 3.

6.1 Metallicity

NGC 7479 has a bright B-band absolute magnitude of $M_B = -21.64$.[11] Using the calibration of Boissier & Prantzos (2009) suggests a supersolar oxygen abundance of $12 + \log(\mathrm{O/H}) = 9.09$ dex at the characteristic radius of 0.4 R_{25}.[12] A direct estimate for the host-galaxy metallicity can be obtained from the line fluxes of nebular emission lines in the vicinity of the SN. Actually, many different diagnostics for metallicity can be found in the literature (e.g. McGaugh 1991; Kewley & Dopita 2002; Pettini & Pagel 2004; Pilyugin & Thuan 2005) using various emission-line ratios and calibrations. Different metallicity calibrations also give systematically different results (Ellison, Kewley & Mallén-Ornelas 2005; Modjaz et al. 2008a; Smartt et al. 2009). In this paper, we follow Modjaz et al. and use a range of methods to determine the metallicity.

The strengths of the host-galaxy emission lines were measured in the deep spectrum of SN 2009jf obtained on 2010 July 7 with the WHT and ISIS (see Fig. 15). The measured fluxes are listed in Table 4.

The N2 index calibration of Pettini & Pagel (2004) gives 12+log(O/H) = 8.56 dex, while the O3N2 index by the same authors gives a value of 8.43 dex. Pilyugin & Mattsson (2011) use the NS calibration to give relations for the oxygen abundance 12+log(O/H), and the nitrogen abundance 12+log(N/H). With the measured fluxes near the site of the SN, we derive 8.36 dex for the former and 7.49 dex for the latter. Kobulnicky & Kewley (2004) give an approximation for the average of the KD02 and M91 relations, which gives 12+log(O/H) = 8.67 dex.

The mean of these four values for the metallicity is 8.51 dex, which is between the solar value (8.72 dex; Allende Prieto, Lambert & Asplund 2001) and that of the Large Magellanic Cloud (LMC) (8.35 dex; Hunter et al. 2007) which is considerably smaller than the value obtained with the B-band absolute magnitude of NGC 7479.

[11] HyperLEDA; http://leda.univ-lyon1.fr/

[12] The R25 radius is the radius of the 25 mag arcsec^2 B-band isophote.

Table 3. Main parameters for SN 2009jf and its host galaxy.

Parent galaxy	NGC 7479
Galaxy type	SBbc[a]
RA (2000)	$23^h04^m52\overset{s}{.}98$
Dec. (2000)	$+12^\circ19'59\overset{''}{.}5$
Recession velocity	2443 (km s^{-1}) [a]
Distance modulus ($H_0 = 72$)	32.65 ± 0.10 mag
$E(B-V)_{7479}$	0.0–0.1 mag
$E(B-V)_{\mathrm{MW}}$	0.112 mag[b]
Offset from nucleus	$53\overset{''}{.}8$ W, $36\overset{''}{.}5$ N
Explosion epoch (JD)	245 5099.5 ± 1.0 (2009 September 25)

[a]LEDA, velocity corrected for Local Group infall on to the Virgo cluster.
[b]Schlegel et al. (1998).

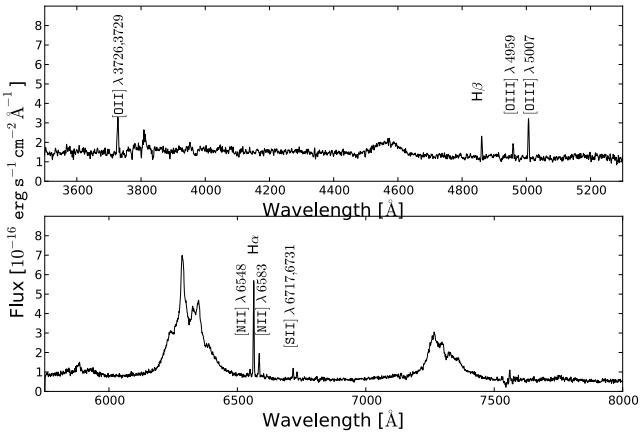

Figure 15. Host-galaxy emission lines in the late-time spectrum of SN 2009jf at +266 d from B-band maximum.

Table 4. Nebular emission lines seen in the spectrum of 2010 July 7. The spectrum has been corrected for host and Galactic extinction, and the fluxes of all emission lines of interest were measured subtracting the continuum and fitting a Gaussian to the line using IRAF.

Species	Wavelength (Å)	Flux (10^{-17}) (erg s^{-1} cm^{-2})
[O II]	372 629	183
Hβ	4861	58
[O III]	4959	45
[O III]	5007	125
[N II]	6548	20
Hα	6563	273
[N II]	6583	68
[S II]	6717	31
[S II]	6731	25

6.2 The progenitor of SN 2009jf

To search for possible evidence of the progenitor, the post-explosion NaCo K_S-band image from 2009 October was aligned with the stacked pre-explosion WFPC2 $F814W$ image. 12 sources com-

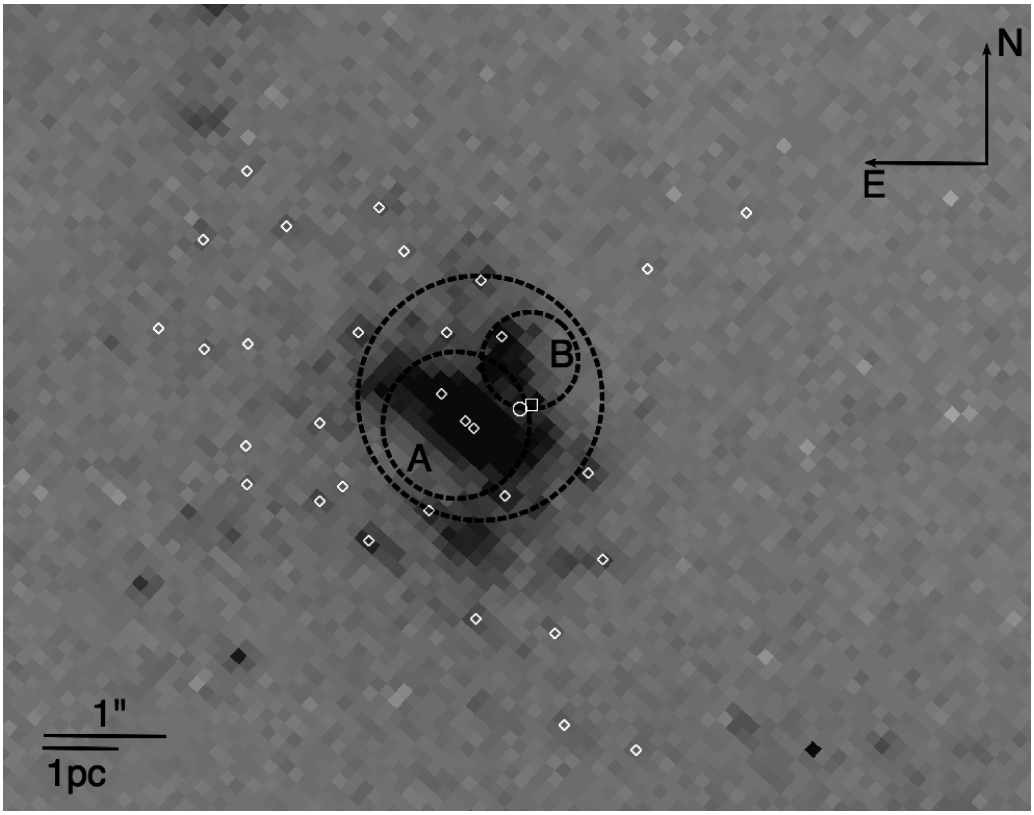

Figure 16. The *HST*+WFPC2 *F*569*W* image of the location of SN 2009jf. Scale and orientation are indicated. The position of the SN, as determined from the post-explosion NaCo image, is located with a white circle. The radius of the circle corresponds to the 57 mas uncertainty in the SN coordinates and the geometric transformation. All sources detected by HSTPHOT within a distance of 31 pixels of the SN location (corresponding to a 500 pc radius at the distance of NGC 7479) at the 3σ level in both filters are indicated with white diamonds. The source located close to the SN in the *F*569*W* filter is indicated with a white square. The regions used for aperture photometry of the complexes as discussed in the text are indicated with dashed circles, and labelled accordingly.

mon to both images were identified and their positions were measured accurately with the IRAF PHOT task. Using the resulting list of matched pixel coordinates, we derived a geometrical transformation[13] between the two images, using IRAF GEOMAP. The rms error in the transformation was found to be 0.573 WF pixels or 57 mas.

The position of the SN was measured in the NaCo image using the three different centring algorithms in IRAF PHOT, all of which agreed to within ∼5 mas. The mean of the three positions was taken as the SN position, this was then transformed to the pixel coordinates of the WFPC2 *F*814*W*-filter image.[14] The SN is in a crowded region, dominated by two bright complexes (A and B) one of which appears elongated (see Fig. 16). We also aligned the *F*569*W* image using the same procedure.[15]

While the SN is not coincident with either of the two complexes A and B, an association is still plausible. The SN is ∼5 pixels (0.5 arcsec) from the brightest pixels in A and B. At the distance of NGC 7479, and scaling by $4/\pi$ to account for projection, this corresponds to ∼100 pc. If we assume a velocity of 100 km s^{-1} for the progenitor, it could traverse this distance in ∼1 Myr. As this is a factor of 10 less than the lifespan of a single 25 $M_\odot$ star (Fig. 18), the progenitor could well be associated with either region A or B (or indeed be unrelated to both).

The HSTPHOT package (Dolphin 2000) was used to produce photometry of all sources detected in the region of the SN.[16] HSTPHOT was then run separately for the co-added *F*569*W* and *F*814*W* filter images with a detection threshold of 3σ.

A colour–magnitude diagram of all sources detected by HSTPHOT in both filters, within ∼500 pc of SN 2009jf, is shown in Fig. 17. As can be seen, there are no evolved red sources detected in both filters, and indeed the population appears quite blue, which is indicative of a young and massive stellar population. While the population of detected sources appears blue, the limiting magnitudes of the images likely prevent us from detecting most of the evolved red supergiant population, or the main sequence below about 20–30 $M_\odot$. As such, it is difficult to provide an estimate of an age for the surrounding stellar population. It is likely that most objects brighter than −8.5 are unresolved, compact clusters. Furthermore, the region is similar to the 50–300 pc sized star-forming complexes that are common in late-type spirals (Bastian et al. 2005). Such complexes typically contain compact star clusters of <10 pc diameter, which are likely

[13] As a small number of common sources were used for the alignment, we restricted the transformation to rotation, scaling and translation only.

[14] The derived pixel positions of the SN in the coordinates of u2z00103t.c0f.fits are 471.55 and 134.53.

[15] The *F*569*W* image was found to be offset from the *F*814*W* image by (−0.05, −0.43) WF pixels in *x* and *y* respectively, this offset has been corrected for in all of the following.

[16] We used the pre-processing programs that accompany HSTPHOT to remove cosmic rays and hot pixels (MASK, CRMASK, HOTPIXELS), to combine the individual exposures in each filter (COADD) and to measure the sky background (GETSKY).

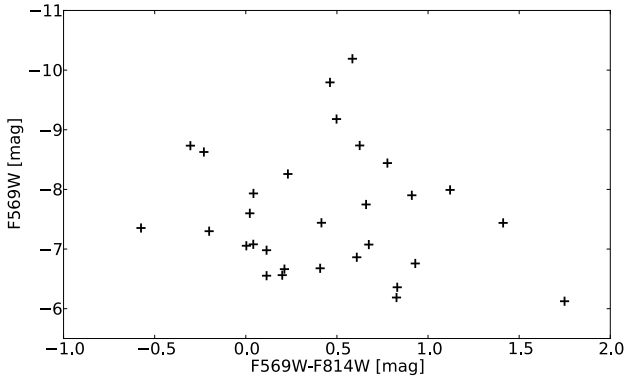

Figure 17. All sources detected by HSTPHOT above the 3σ level in both the $F569W$ and $F814$ filters. Magnitudes have been corrected for the distance of NGC 7479 and for Milky Way extinction, but not for extinction in the host. Furthermore, we have made no attempt to separate out sources which are poorly fitted by a PSF, and are hence likely unresolved clusters. Indeed, any source with an absolute magnitude brighter than -8.5 mag is likely a cluster rather than a single star.

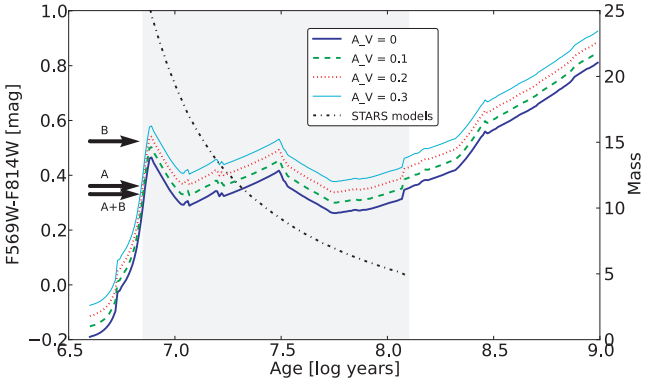

Figure 18. Padova integrated model $F569W - F814W$ colours of a stellar population (on the left y-axis) are plotted against the age of the population for a range of extinctions. The observed colours of regions A and B, together with the total colour of the entire region (A+B), are indicated with arrows; these values have been corrected for Milky Way extinction only. The range of population ages (approximately 10–100 Myr) which are consistent with the cluster colours is indicated by the shaded region. Unfortunately, there is a strong degeneracy in the $F569W - F814W$ colour of the models. On the right y-axis, the zero-age main-sequence (ZAMS) mass of single stars from the STARS code are plotted against their lifespan. A population age of 10 Myr is consistent with a progenitor mass of 25 $M_\odot$, while for an older population the progenitor must be less massive, likely $\sim$8 $M_\odot$.

to host coeval populations themselves. However, the whole star-forming complex may have a significant age spread (see discussion in Crockett et al. 2008). The closest source detected by HSTPHOT is 66 mas (10 pc) away from the nominal SN position in the $F569W$ ($m_{F569W} = 23.75$). With an absolute magnitude of $M_{F569W} = -9.25$, this is likely to be a compact cluster. The host region of SN2009jf is quite similar to that of SN2007gr (Crockett et al. 2008), with the SN being close to (but not exactly coincident) with a compact cluster and contained with a larger star-forming complex.

We can also attempt to estimate the age of the population by comparing the observed colours of the region to models. If we can determine the age of the A and B regions, then we can infer the most massive stars which would be still extant at that time. We have performed simple aperture photometry on the $F569W$ and $F814W$ filter WFPC2 images on the regions indicated A and B in Fig. 16. Using the revised zero-points of Dolphin (2009), and correcting for Milky Way extinction, we find the colours of regions A and B to be $M_{F569W-F814W} = 0.36$ and 0.52 mag, respectively. In a large aperture encompassing both regions (also indicated in Fig. 16 with a dashed circle), we find a colour of $M_{F569W-F814W} = 0.33$ mag, which is reassuring as this is a similar colour to region A, which contributes most of the flux. We have no constraint on the internal extinction in the complexes, so we will regard these colours as upper limits on the true colours, which are likely bluer.

We have used the Padova stellar population models[17] (Girardi et al. 2002; Marigo et al. 2008) to create a table of integrated magnitudes for a single stellar population, at a metallicity appropriate to the site of SN 2009jf ($Z = 0.012$), and in the WFPC2 filter system. The Padova model colours are shown as a function of age in Fig. 18, together with the lifetimes of massive stars as found from the STARS evolutionary code (Stancliffe & Eldridge 2009). The degeneracy in the $M_{F569W-F814W}$ colour versus age plot precludes us from determining the age for the clusters. Region A is consistent with an unreddened population of stars with a maximum progenitor mass somewhere between 8 and 25 $M_\odot$. Complex B is redder which implies an older age. But the degeneracy between age and extinction prevents a useful determination. For example, a moderate amount of internal extinction would make the age range consistent with a 8–25 $M_\odot$ population. Unfortunately, the compact cluster which is closest to the progenitor position is detected only in the $F569W$ filter, and so we cannot constrain its age, beyond the fact that it is blue, and hence presumably among the younger objects in the region. As for the progenitor of SN2007gr and its possible host cluster, future observations of the region with *HST* in the U and B bands could age date the cluster.

We also present an Hα image of NGC 7479, which was obtained on 1996 September 13 with the Prime Focus Cone Unit + CCD on the Isaac Newton Telescope. This deep image consisted of an 1800-s exposure taken with the $H626$ filter (Hα) and another 1800-s exposure taken with the $H712$ filter to allow for removal of continuum light. The HOTPANTS package (A. Becker) was used to subtract the continuum image from the Hα image. The Hα flux does not appear to be from a point source, but is rather spread out over several pixels at the southern end of the complexes. The SN position in the Hα image was determined by alignment to a Liverpool Telescope r'-band image, and is found to be on the edge of this region of Hα flux (as shown in Fig. 13).

In conclusion, the environment of the SN clearly displays signs of recent star formation, with a strong Hα flux and integrated colours which are consistent with a young, massive stellar population. A colour–magnitude diagram of sources within a radius of 500 pc of the SN indicates a young population, with no detections of the red supergiants which may be expected in a slightly more evolved population. The progenitor is close to, but not coincident with, two regions which we have termed A and B. Unfortunately we cannot distinguish between a high-mass ($\sim$25 $M_\odot$) or low-mass ($\sim$10 $M_\odot$) progenitor on the basis of the age of the clusters due to the degeneracy in the age–colour relation. However, on the basis of the Hα flux and the surrounding blue stellar population, together with the characteristics of the SN, we consider the high-mass channel more likely. Future observations after the SN has faded may help to better address this issue.

[17] http://stev.oapd.inaf.it/cmd

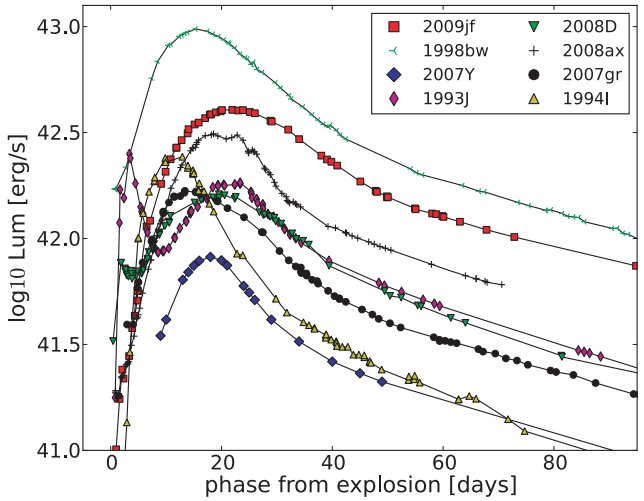

Figure 19. The bolometric light curve of SN 2009jf compared with those of other core-collapse SNe. References for each SN: SN 2009jf: this work; SN 1998bw: $E(B-V) = 0.06$ mag, $\mu = 32.76$ mag, phot. data – Patat et al. (2001); SN 1994I: $E(B-V) = 0.04$ mag, $\mu = 29.60$ mag (Sauer et al. 2006), phot. data – Richmond et al. (1996); SN 1993J: $E(B-V) = 0.079$ mag (Barbon et al. 1995), $\mu = 27.8$ mag (Freedman et al. 1994), phot data – Barbon et al. (1995); SN 2008D: $E(B-V) = 0.65$, $\mu = 32.29$ mag (Mazzali et al. 2008), phot. data – Mazzali et al. (2008); Modjaz et al. (2009); SN 2007gr: $E(B-V) = 0.092$ mag, $\mu = 29.84$ mag, phot. data – Valenti et al. (2008b); Hunter et al. (2009); SN 2008ax: $E(B-V) = 0.40$ mag (Taubenberger et al. 2011), $\mu = 29.92$ mag (Pastorello et al. 2008), phot. data – Pastorello et al. (2008); Taubenberger et al. (2011); SN 2007Y: $E(B-V) = 0.112$ mag, $\mu = 31.13$ mag, phot. data – Stritzinger et al. (2009).

7 BOLOMETRIC LIGHT CURVE OF SN 2009jf

The bolometric light curve of a SN is a powerful tool to validate model predictions. It is well known that, starting from ∼1 week past explosion, the light curve of a non-interacting stripped-envelope SN is mainly determined by the amount of nickel synthesized during the explosion, together with the amount of ejected material and the kinetic energy (Arnett 1980, 1982). As a first-order approximation to the true bolometric luminosity, we integrated the SN emission in the spectral window accessible from ground, from the UV atmospheric cut-off to the NIR (*JHK*).[18] All magnitudes were then converted to fluxes[19] and integrated from U to K using Simpson's rule. The resulting bolometric light curve is shown in Fig. 19 together with the bolometric light curves of other stripped-envelope SNe. SN 2009jf is one of the brightest SNe Ib observed to date. At 20.5 d after explosion, it reached a maximum luminosity of $\log_{10}L = 42.62 \pm 0.05$ erg s^{-1}, in between the Type Ic GRB-SN 1998bw and SN 2008ax. The light curve of SN 2009jf evolves quite slowly, only reaching the radioactive tail around 50 d after explosion. The slope of the tail is then 0.0133 mag d^{-1}, which is faster than the cobalt decay time-scale.

Valenti et al. (2008a) developed a toy model in order to compute a first-order estimate of the main physical parameters that shape the bolometric light curve (see also Chatzopoulos, Wheeler & Vinko 2009): $M_{56\rm Ni}$, $M_{\rm ej}$ and $E_{\rm k}$. The toy model is based on very simple approximations (Arnett 1982; Cappellaro et al. 1997; Clocchiatti & Wheeler 1997), dividing the light curve into an optically thick (photospheric) and an optically thin (nebular) phase. Adopting a photospheric velocity at maximum of 11000 km s^{-1} and an optical opacity of $k_{\rm opt} = 0.06$, we obtained the following parameters: $M_{56\rm Ni} = 0.23 \pm 0.02\,{\rm M}_\odot$, $M_{\rm ej} = 5$–$7\,{\rm M}_\odot$ and $E_{\rm k} = 5.5$–$10.6 10^{51}$ erg. In Appendix B, we report in more detail on the toy model as applied to the case of SN 2009jf and other SNe Ib, along with some caveats. The ejected mass we find for SN 2009jf is comparable with those obtained for other massive SNe Ib (SN 2008D, Mazzali et al. 2008; Tanaka et al. 2009; SN 1999dn, Benetti et al. 2011) and for some massive and energetic SNe Ic. The kinetic energy obtained is quite high. This is not surprising however, since our toy model also seems to overestimate the kinetic energy for other SNe Ib. The true kinetic energy of SN 2009jf is likely close to the lower edge of our range. Nevertheless, the values we find for the kinetic energy and ejected mass are consistent with those of Sahu et al. (2011). The ejected nickel mass of Sahu et al. ($0.17 \pm 0.03\,{\rm M}_\odot$) is slightly smaller than our value, most likely because they did not include the IR contribution in their bolometric light curve.[20]

8 DISCUSSION

In the last 5 years, good data sets have been published for several SNe Ib (SN 2007Y, Stritzinger et al. 2009; SN 2008D, Mazzali et al. 2008; Soderberg et al. 2008; Malesani et al. 2009; Modjaz et al. 2009; SN 2008ax, Pastorello et al. 2008; Chornock et al. 2010; Taubenberger et al. 2011; SN 2009jf, Sahu et al. 2011, this work). These data allow us for the first time to make comparisons between the different stripped-envelope SNe subtypes. The broad light curves and the evidence that some SNe Ib are quite luminous and energetic suggest that these explosions do not always release the canonical 10^{51} erg, as often assumed.

In fact, SN 2007Y, one of the faintest and least massive He-rich SNe (Stritzinger et al. 2009), ejected $\sim 2\,{\rm M}_\odot$ of material once the He ($1.5\,{\rm M}_\odot$) and residual H ($0.1\,{\rm M}_\odot$) layers (Maurer et al. 2010) are taken into account.[21] In this context, SN 2009jf is one of the most energetic and massive SNe Ib known to date.

From Fig. 19, it is clear that, while some He-poor SNe (e.g. SNe 1998bw, 2007gr) show an asymmetric peak (with a faster rise than decay), all the He-rich SNe show a slow rise to maximum. In Fig. 20 we show the rise times for a sample of stripped-envelope SNe. In the sample of published SNe Ib, we have tried to include only SNe with reasonable information on the explosion epoch (early discovery or good pre-discovery limit) and good data coverage. SN 1983N has also been included because of the early V-band discovery, even though the light curve coverage is not ideal. Only two SNe Ic, with data published, have been monitored soon after the explosion, although for some broad-lined SNe Ic the explosion epoch is well constrained by the associated X-ray flash or GRB. We have excluded stripped-envelope SNe for which there is evidence of circumstellar interaction, as interaction will increase the luminosity of the SN. We also excluded the new class of ultra-bright SNe (Quimby et al. 2011; Pastorello et al. 2010) that share some similarities with SNe Ic (Pastorello et al. 2010), for which a flux contribution to the

[18] Photometric data in the Sloan filters were transformed from the AB to Vega system (Holberg & Bergeron 2006).

[19] The zero-points for the conversion have been computed by integrating the spectrum of Vega with the Landolt and Sloan filters (Buser & Kurucz 1978; Gunn et al. 1998).

[20] Their overestimate of the radioactive tail magnitude does not change their nickel mass estimate as this is mainly based on the SN magnitude at maximum light.

[21] Stritzinger et al. (2009) found that excluding He and H, the ejected mass of SN 2007Y was $\sim 0.45\,{\rm M}_\odot$.

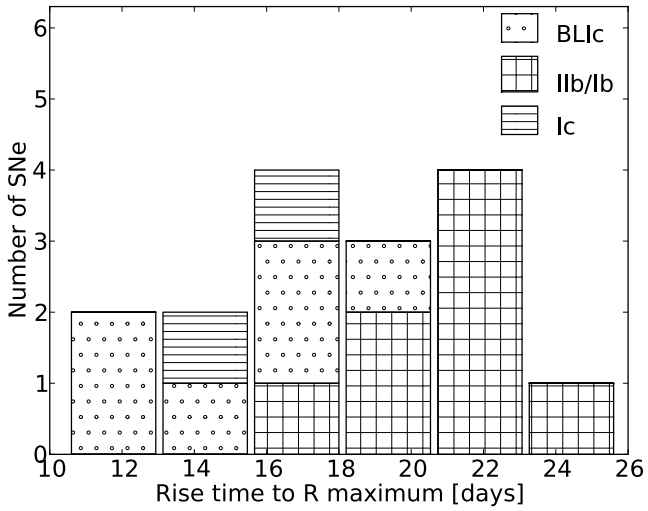

Figure 20. The rise times of a sample of stripped-envelope SNe. References for each SN: 1998bw (from GRB 980425, Soffitta et al. 1998); 1994I (modelling, Sauer et al. 2006); 2003jd (pre-explosion limit, Valenti et al. 2008a); 1999ex (early discovery, Stritzinger et al. 2002); 2002ap (modelling, Mazzali et al. 2002); 1997ef (modelling, Mazzali, Iwamoto & Nomoto 2000); 2006aj (from GRB060218, Cusumano et al. 2006); 1993J (early discovery, Lewis et al. 1994); 2007gr (good pre-explosion limit, Valenti et al. 2008b); 2008D (from *Swift* detection, Berger & Soderberg 2008); 2008ax (pre-discovery limit, Pastorello et al. 2008); 1996cb (1 day from early discovery, Qiu et al. 1999); 1983N: (1 day from early discovery, Richtler & Sadler 1983); 2007Y (1 day from early discovery, Stritzinger et al. 2009); 2009bb (good pre-explosion limit, Pignata et al. 2011).

light curve due to interaction has also been proposed (Blinnikov & Sorokina 2010). These SNe show rise times of up to ∼100 d, and may have an origin different to *normal* Ic SNe.

Even though the longer rise times for He rich SNe are clearly apparent, we must consider the possibility that this is a selection effect. SNe Ib are quite rare, and slowly evolving/rising SNe Ib are easier to discover at an earlier phase than fast rising SNe Ib. However, our findings are confirmed by Drout et al. (2010) who recently presented an extended set of stripped-envelope light curves in which there are no fast rising SNe Ib, and SN 1994I is the only fast evolving stripped-envelope SN.

Recently, several fast evolving stripped-envelope SNe have been discovered (or recovered in archival data), but unfortunately none of them has been well covered in the pre-maximum phase (e.g. SN 2008ha, Valenti et al. 2009; Foley et al. 2009; SN 2005E, Perets et al. 2010; SN 2002bj, Poznanski et al. 2010; SN 2005cz, Kawabata et al. 2010). It is also highly debated whether they are core-collapse SNe, thermonuclear explosions in a *non-canonical* Ia scenario, or even new explosion channels. If we believe that these fast evolving stripped-envelope SNe are not core-collapse explosions, we will conclude that, with the exception of SN 1994I, all stripped-envelope SNe ejected at least 2 $M_\odot$ of material.

The large ejected mass (3–7 $M_\odot$) and large oxygen mass (the latter reported by Sahu et al. 2011) of SN2009jf could be explained by the explosion of a 5–9 $M_\odot$ CO star (assuming 1.5 $M_\odot$ neutron star remnant). The WC[22] population in the LMC have pre-SN masses between 6 and 18 $M_\odot$ (Crowther et al. 2002). A 5–9 $M_\odot$ CO star could originate in a single massive progenitor of $M_{\rm ZAMS} > 35\,M_\odot$ (Eldridge & Tout 2004; Georgy et al. 2009) with radiative driven mass loss, suggesting that a massive WR star (with a low He residual mass) is plausible. Equally a lower mass star which has been stripped of its envelope through binary transfer is also possible – the CO core mass of a 20 $M_\odot$ star is about 5 $M_\odot$ in the STARS models (Eldridge & Tout 2004). The analysis of the progenitor environment cannot distinguish between these two, as the age of the stellar population in the vicinity of the SN progenitor is not constrained well enough to determine a star formation age. The fact that the SN is very close to a compact star cluster suggests that an age determination of that cluster could provide further constraints, if UV data are obtained once the SN has faded.

The detection of relatively weak He at high velocity and the spectral similarity with the He-poor SN 2007gr suggest the presence of only a small amount of He in the ejecta of SN 2009jf. However, this conclusion needs to be confirmed by detailed spectral modelling of SN 2009jf.

The profile of [O I] λλ6300, 6364 is suggestive of an asymmetric explosion with an off-axis dense core with clumps. Similar conclusions can be drawn for the magnesium and calcium distribution by comparing their line profiles to that of oxygen. While a similar profile is expected for Mg I] and O I as they come from similar regions in the ejecta; [Ca II] λλ7291, 7324 should form in the inner part of the ejecta where silicon is more abundant or in the outer layer of He (Fransson & Chevalier 1989). The similar profile for the three lines could indicate that mixing is an important factor in the explosion of SN 2009jf.

9 SUMMARY

In this paper we have presented optical and IR photometry and spectroscopy of SN 2009jf spanning from ∼20 d before *B*-band maximum to 1 year after maximum.

We have shown that SN 2009jf is a slowly evolving, massive and energetic stripped-envelope SN which retained only a small part of its He layer at the moment of explosion. The SN exploded in a young stellar environment, and the progenitor is likely a massive star >25–30 $M_\odot$ as suggested by Sahu et al. (2011). Furthermore, the similarity with the SN Ic 2007gr suggests a similar progenitor for at least some SNe Ib and Ic. The nebular spectra of SN 2009jf are consistent with an asymmetric explosion with an off-centre dense core.

We have also shown that He-rich SNe appear to have longer rise times than other stripped-envelope SNe. However, this should be treated as a preliminary result, and needs to be verified with a larger sample of stripped-envelope SNe, while carefully accounting for all possible systematic biases.

ACKNOWLEDGMENTS

We thank the anonymous referee for helpful suggestions. SV is grateful to H. Wang for hospitality at the UCLA. GP acknowledges support by the Proyecto FONDECYT 11090421. SB, EC, MTB, FB, PAM and MT are partially supported by the PRIN-INAF 2009 with the project *Supernovae Variety and Nucleosynthesis Yields*. GP, MH and JM acknowledge support from the Millennium Center for Supernova Science through grant P06-045-F funded by 'Programa Bicentenario de Ciencia y Tecnología de CONICYT', 'Programa Iniciativa Cientifica Milenio de MIDEPLAN', from Centro de Astrofisica FONDAP 15010003, and by Fondecyt through grant 1060808 from the Center of Excellence in Astrophysics and Associated Technologies (PFB 06). ST acknowledges support by the TRR 33 'The Dark Universe' of the German Research Foundation. SM acknowledges support from the Academy of Finland

[22] Carbon dominated WR stars.

(project 8120503). EK acknowledges financial support from the Finnish Academy of Science and Letters (Vilho, Yrjö and Kalle Väisälä Foundation). This paper is based on observations made with the following facilities: ESO Telescopes at the La Silla and Paranal Observatories under programme IDs 184.D-1151, 085.D-0750 and 386.D-0126, the Italian National Telescope Galileo (La Palma), the 1.82-m Copernico telescope of the Asiago Observatory (Italy), the William Herschel (La Palma), Liverpool Telescope (La Palma), Nordic Optical Telescope (La Palma), AlbaNova Telescope (Sweden), Prompt telescopes (Chile), Calar Alto (Spain). We thank Genoveva Micheva for help with the observations. We are grateful to the staff at all of the telescopes for their assistance. This paper makes use of data obtained from the Isaac Newton Group Archive which is maintained as part of the CASU Astronomical Data Centre at the Institute of Astronomy, Cambridge. Based on observations made with the NASA/ESA *HST*, obtained from the data archive at the Space Telescope Institute. STScI is operated by the association of Universities for Research in Astronomy, Inc. under the NASA contract NAS 5-26555. We thank K. Itagaki for providing us his images of SN 2009jf. This manuscript made use of information contained in the Bright Supernova web pages (maintained by the priceless work of D. Bishop), as part of the Rochester Academy of Sciences (http://www.RochesterAstronomy.org/snimages). This publication makes use of data products from the Two Micron All-Sky Survey, which is a joint project of the University of Massachusetts and the Infrared Processing and Analysis Center/California Institute of Technology, funded by the National Aeronautics and Space Administration and the National Science Foundation.

REFERENCES

Alard C., 2000, A&AS, 144, 363
Alard C., Lupton R. H., 1998, ApJ, 503, 325
Allende Prieto C., Lambert D. L., Asplund M., 2001, ApJ, 556, L63
Anderson J. P., James P. A., 2009, MNRAS, 399, 559
Anderson J. P., Covarrubias R. A., James P. A., Hamuy M., Habergham S. M., 2010, MNRAS, 407, 2660
Arnett W. D., 1980, ApJ, 237, 541
Arnett W. D., 1982, ApJ, 253, 785
Barbon R., Benetti S., Cappellaro E., Patat F., Turatto M., Iijima T., 1995, A&AS, 110, 513
Bastian N., Gieles M., Lamers H. J. G. L. M., Scheepmaker R. A., de Grijs R., 2005, A&A, 431, 905
Benetti S. et al., 2011, MNRAS, 411, 2726
Berger E., Soderberg A. M., 2008, GRB Coordinates Network, 7159, 1
Blinnikov S. I., Sorokina E. I., 2010, preprint (arXiv:1009.4353)
Boissier S., Prantzos N., 2009, A&A, 503, 137
Branch D. et al., 2002, ApJ, 566, 1005
Branch D., Jeffery D. J., Young T. R., Baron E., 2006, PASP, 118, 791
Brown P. J. et al., 2010, ApJ, 721, 1608
Buser R., Kurucz R. L., 1978, A&A, 70, 555
Cappellaro E., Mazzali P. A., Benetti S., Danziger I. J., Turatto M., della Valle M., Patat F., 1997, A&A, 328, 203
Chatzopoulos E., Wheeler J. C., Vinko J., 2009, ApJ, 704, 1251
Chevalier R. A., Soderberg A. M., 2010, ApJ, 711, L40
Chornock R. et al., 2010, ApJL, submitted (arXiv:1004.2262)
Chugai N. N., 1992, SvA, 18, L239
Clocchiatti A., Wheeler J. C., 1997, ApJ, 491, 375
Crockett R. M., 2009, PhD thesis, Queen's University
Crockett R. M. et al., 2008, ApJ, 672, L99
Crowther P. A., Dessart L., Hillier D. J., Abbott J. B., Fullerton A. W., 2002, A&A, 392, 653
Cusumano G., Barthelmy S., Gehrels N., Hunsberger S., Immler S., Marshall F., Palmer D., Sakamoto T., 2006, GRB Coordinates Network, 4775, 1
Dolphin A. E., 2000, PASP, 112, 1383
Drout M. R. et al., 2010, ApJ, submitted (arXiv:1011.4959)
Eldridge J. J., Tout C. A., 2004, MNRAS, 353, 87
Eldridge J. J., Izzard R. G., Tout C. A., 2008, MNRAS, 384, 1109
Ellison S. L., Kewley L. J., Mallén-Ornelas G., 2005, MNRAS, 357, 354
Elmhamdi A., Danziger I. J., Branch D., Leibundgut B., Baron E., Kirshner R. P., 2006, A&A, 450, 305
Filippenko A. V., Shields J. C., Richmond M. W., 1990, IAU Circ., 5069, 1
Filippenko A. V., Li W. D., Treffers R. R., Modjaz M., 2001, in Paczynski B., Chen W.-P., Lemme C., eds, ASP Conf. Ser. Vol. 246, IAU Colloq. 183, Small Telescope Astronomy on Global Scales. Astron. Soc. Pac., San Francisco, p. 121
Foley R. J. et al., 2009, AJ, 138, 376
Fransson C., Chevalier R. A., 1989, ApJ, 343, 323
Freedman W. L. et al., 1994, ApJ, 427, 628
Fryer C. L. et al., 2007, PASP, 119, 1211
Georgy C., Meynet G., Walder R., Folini D., Maeder A., 2009, A&A, 502, 611
Girardi L., Bertelli G., Bressan A., Chiosi C., Groenewegen M. A. T., Marigo P., Salasnich B., Weiss A., 2002, A&A, 391, 195
Gunn J. E. et al., 1998, AJ, 116, 3040
Hamuy M. et al., 2002, AJ, 124, 417
Holberg J. B., Bergeron P., 2006, AJ, 132, 1221
Hoot J. E., 2007, Soc. Astron. Sci. Ann. Symp., 26, 67
Hunter I. et al., 2007, A&A, 466, 277
Hunter D. J. et al., 2009, A&A, 508, 371
Itagaki K., Kaneda H., Yamaoka H., 2009, Cent. Bureau Electron. Telegrams, 1955, 3
Kasliwal M. M., Howell J. L., Fox D. B., Quimby R., Gal-Yam A., 2009, Cent. Bureau Electron. Telegrams, 1955, 1
Kawabata K. S. et al., 2010, Nat, 465, 326
Kewley L. J., Dopita M. A., 2002, ApJS, 142, 35
Kobulnicky H. A., Kewley L. J., 2004, ApJ, 617, 240
Laine S., 2008, ApJ, 673, 128
Laine S., Beck R., 2005, BAAS, 37, 1392
Laine S., Gottesman S. T., 1998, MNRAS, 297, 1041
Landolt A. U., 1992, AJ, 104, 340
Leibundgut B., Kirshner R. P., Pinto P. A., Rupen M. P., Smith R. C., Gunn J. E., Schneider D. P., 1991, ApJ, 372, 531
Leloudas G. et al., 2011, A&A, 530, A95
Lewis J. R. et al., 1994, MNRAS, 266, L27
Li W., Jha S., Filippenko A. V., Bloom J. S., Pooley D., Foley R. J., Perley D. A., 2006, PASP, 118, 37
Li W., Cenko S. B., Filippenko A. V., 2009, Cent. Bureau Electron. Telegrams, 1952, 1
Lucy L. B., 1991, ApJ, 383, 308
McGaugh S. S., 1991, ApJ, 380, 140
Maeda K., Nomoto K., Mazzali P. A., Deng J., 2006, ApJ, 640, 854
Maeda K. et al., 2008, Sci, 319, 1220
Malesani D. et al., 2009, ApJ, 692, L84
Marigo P., Girardi L., Bressan A., Groenewegen M. A. T., Silva L., Granato G. L., 2008, A&A, 482, 883
Maurer I., Mazzali P. A., Taubenberger S., Hachinger S., 2010, MNRAS, 409, 1441
Mazzali P. A., Iwamoto K., Nomoto K., 2000, ApJ, 545, 407
Mazzali P. A., Nomoto K., Patat F., Maeda K., 2001, ApJ, 559, 1047
Mazzali P. A. et al., 2002, ApJ, 572, L61
Mazzali P. A. et al., 2005, Sci, 308, 1284
Mazzali P. A. et al., 2008, Sci, 321, 1185
Milisavljevic D., Fesen R. A., Gerardy C. L., Kirshner R. P., Challis P., 2010, ApJ, 709, 1343
Modjaz M. et al., 2008a, AJ, 135, 1136
Modjaz M., Kirshner R. P., Blondin S., Challis P., Matheson T., 2008b, ApJ, 687, L9
Modjaz M. et al., 2009, ApJ, 702, 226
Modjaz M., Kewley L., Bloom J. S., Filippenko A. V., Perley D., Silverman J. M., 2011, ApJ, 731, L4
Pastorello A. et al., 2008, MNRAS, 389, 955
Pastorello A. et al., 2010, ApJ, 724, L16

Patat F. et al., 2001, ApJ, 555, 900
Pennypacker C., Perlmutter S., Marvin H., 1990, IAU Circ., 5063, 1
Perets H. B. et al., 2010, Nat, 465, 322
Pettini M., Pagel B. E. J., 2004, MNRAS, 348, L59
Phillips M. M., Lira P., Suntzeff N. B., Schommer R. A., Hamuy M., Maza J., 1999, AJ, 118, 1766
Pignata G. et al., 2008, MNRAS, 388, 971
Pignata G. et al., 2011, ApJ, 728, 14
Pilyugin L. S., Mattsson L., 2011, MNRAS, 412, 1145
Pilyugin L. S., Thuan T. X., 2005, ApJ, 631, 231
Podsiadlowski P., Joss P. C., Hsu J. J. L., 1992, ApJ, 391, 246
Poznanski D. et al., 2010, Sci, 327, 58
Prieto J. L., Stanek K. Z., Beacom J. F., 2008, ApJ, 673, 999
Qiu Y., Li W., Qiao Q., Hu J., 1999, AJ, 117, 736
Quimby R. M. et al., 2011, Nat, 474, 487
Reichart D. et al., 2005, Nuovo Cimento C Geophys. Space Phys. C, 28, 767
Richmond M. W. et al., 1996, AJ, 111, 327
Richtler T., Sadler E. M., 1983, A&A, 128, L3
Sahu D. K., Anupama G. C., Gurugubelli U. K., 2009, Cent. Bureau Electron. Telegrams, 1955, 2
Sahu D. K., Gurugubelli U. K., Anupama G. C., Nomoto K., 2011, MNRAS, 413, 2583
Sauer D. N., Mazzali P. A., Deng J., Valenti S., Nomoto K., Filippenko A. V., 2006, MNRAS, 369, 1939
Schlegel D. J., Finkbeiner D. P., Davis M., 1998, ApJ, 500, 525
Smartt S. J., 2009, ARA&A, 47, 63
Smartt S. J., Eldridge J. J., Crockett R. M., Maund J. R., 2009, MNRAS, 395, 1409
Smith J. A. et al., 2002, AJ, 123, 2121
Soderberg A. M. et al., 2008, Nat, 453, 469
Soffitta P. et al., 1998, IAU Circ., 6884, 1
Spyromilio J., Pinto P. A., 1991, in Danziger I. J., Kja K., eds, Proc. ESO/EIPC Workshop, Supernova 1987A and other Supernovae. ESO, Garching, p. 423
Stancliffe R. J., Eldridge J. J., 2009, MNRAS, 396, 1699
Stanishev V., 2007, Astron. Nachr., 328, 948
Stritzinger M. et al., 2002, AJ, 124, 2100
Stritzinger M. et al., 2009, ApJ, 696, 713
Tanaka M. et al., 2009, ApJ, 692, 1131
Taubenberger S. et al., 2006, MNRAS, 371, 1459
Taubenberger S. et al., 2009, MNRAS, 397, 677
Taubenberger S. et al., 2011, MNRAS, 413, 140
Turatto M., Benetti S., Cappellaro, 2003, in Hillebrandt W., Leibundgut B., eds, Proc. ESO/MPA/MPE Workshop, From Twilight to Highlight: The Physics of Supernovae. Springer, Berlin, p. 200
Valenti S. et al., 2008a, MNRAS, 383, 1485
Valenti S. et al., 2008b, ApJ, 673, L155
Valenti S. et al., 2009, Nat, 459, 674

APPENDIX A: DATA REDUCTION

The *Swift* data were reduced using the *Swift* pipeline and colour corrected using the recipe of Li et al. (2006). The data from the Prompt telescopes were pre-reduced by the MCSS group, while for those from the robotic Liverpool+RATCAM telescope, we used the dedicated pipeline. All the other data were spectroscopically and photometrically pre-reduced with the QUBA pipeline.[23] The pre-reduction in the QUBA pipeline (bias, trim and flat-field correction) is performed using PYTHON PYRAF scripts. The magnitude is measured with a PSF-fitting technique (using DAOPHOT). Template subtraction is also implemented using SREGISTER package within IRAF to register the images and ISIS MRJPHOT[24] to subtract an image without the SN to the images with the SN. In the case of SN 2009jf, the SN magnitudes have been measured without using template subtraction for all the data from discovery to 3 weeks after the *B*-band maximum. For these epochs, the SN was bright enough to neglect the contamination from the close-by clusters. The rest of the data were measured after the subtraction of archival template images acquired prior to the SN explosion. A comparison of the SN magnitude as measured with and without template subtraction was made (when the SN was bright) to ensure both methods are consistent. The contamination from the close-by clusters can be neglected until 5 weeks after maximum. After that, the SN magnitude is overestimated by amounts ranging from 0.01 mag in the redder bands at 5 weeks after maximum to 0.5 mag in *B* at 6 months post-maximum, if no template subtraction is performed. Since the contamination is larger in the blue bands, SN magnitudes in the *U*- and *u*-band data were measured after template subtraction at all epochs. In the *z* band, no good templates were found in the archive, and so PSF fitting was used also for the late data points. However, the contamination from the bright clusters should be less than 0.1 mag for our faintest measurement in *z*, and even smaller in the previous epochs.

We found a discrepancy between the *Swift U*-band photometry and the rest of our *U*-band data. The *Swift U*-band photometry using the *Swift* pipeline, colour corrected using the recipe of Li et al. (2006), is initially fainter than our photometry by $\sim$0.1 mag, but becomes brighter by $\sim$0.2 mag as the SN fades. Due to the contamination from the nearby cluster, we re-reduced the *Swift* photometry using the template-subtraction technique and applied an *S*-correction (Pignata et al. 2008) as the *Swift U*-band filter is bluer than the *U* passband in the Landolt system. After making these corrections, the late *Swift U*-band photometry is more consistent with data from other telescopes, although still fainter by $\sim$0.1 mag at maximum light. The strong contamination from the cluster in the *U* band also gives us cause for concern for the *uvw*1 *Swift* data, given the red tail of the *Swift uvw*1 passbands (Brown et al. 2010). The *Swift* data in the *uvm*2 and *uvw*2 filters, as reduced with the *Swift* pipeline, show an almost constant magnitude, which is likely due to the bright cluster and not to the SN. For this reason the *uvm*2 and *uvw*2 magnitudes are not reported in the tables.

Observations of standard fields (Landolt 1992; Smith et al. 2002) during photometric nights were used to calibrate the magnitudes of a local sequence of reference stars (see Fig. 1 and Tables C1 and C2), which were used to calibrate the SN magnitudes obtained under non-photometric conditions. The apparent magnitude of the SN was computed using the zero-point from the local sequence stars, together with a first-order colour correction. The unfiltered images provided by amateur astronomers have been calibrated taking into account the CCD response as a function of wavelength. Some images were acquired with a Bayer filter; these were reduced and calibrated following Hoot (2007) to *BVR* filters in the Landolt system applying only a zero-point.

The *JKH* data have been calibrated using the bright stars from Two Micron All-Sky Survey in the field of SN 2009jf and reported in Table C5. The *UBV* and *uvw*1 *Swift* data are reported in Table C6. The *uvw*1 bands were calibrated to the *Swift* system magnitudes.

The spectroscopic data were reduced using the QUBA spectra reduction tasks, which are based on standard spectroscopic IRAF tasks. A check on the wavelength calibration is performed using

[23] The QUBA pipeline was written by SV for the reduction and analysis of spectrophotometric observations of SNe with the instruments and configurations commonly used within the ELP collaboration.

[24] ISIS is an image subtraction package (Alard & Lupton 1998; Alard 2000); MRJPHOT is the image subtraction task within ISIS.

Table B1. Physical parameters for stripped-envelope SNe derived from models of the bolometric light curves.[a]

SN	v^b_{ph} (km s^{-1})	M_{56Ni}(tot) ($M_\odot$)	M_{ej}(tot) ($M_\odot$)	E_k(tot) (10^{51} erg)	E_k(inner) (10^{51} erg)	M_{56Ni}(inner)/ M_{56Ni}(tot)	$M_{56Ni}(^*)$ ($M_\odot$)	$M_{ej}(^*)$ ($M_\odot$)	$E_k(^*)$ (10^{51} erg)
2009jf	11 000	0.23 ± 0.02	5–7	5.5–10.6	0.21–0.23	0.32–0.42	–	–	–
1999dn	10 100	0.11 ± 0.02	4–6	5–7.5	0.07–0.11	0.3–0.4	–	–	–
2008D	11 000	0.09 ± 0.02	5–7	8–13	0.12–0.18	0.25–0.31	0.07	4.3–6.3	3.5–8.5
2008ax	10 000	0.12 ± 0.02	2–4	2–4	0.16–0.18	0.35–0.45	0.07–0.15	1.9–4.0	0.7–2.1
2007Y	9000	0.04 ± 0.01	1–2	0.7–1.5	0.04–0.08	0.35–0.45	0.06	∼2[c]	∼0.82[d]

[a]The $E(B-V)$ values and the distance moduli are reported in the caption of Fig. 19. For comparison, we report in the last three columns [labelled with (*)] the values of M_{ej}, M_{56Ni} and E_k computed with sophisticated spectral and light-curve modelling [SN 2008ax (Maurer et al. 2010); SN 2007Y (Stritzinger et al. 2009; Maurer et al. 2010) and SN 2008D (Tanaka et al. 2009)].
[b]v_{ph} is the photospheric velocity close to the maximum of the bolometric light curve used as *scale velocity* (Arnett 1982).
[c]This is the total ejected mass including the He and H contribution taken from Stritzinger et al. (2009) and Maurer et al. (2010).
[d]This is the total energy obtained by Stritzinger et al. (2009) considering the total ejected mass (H and He included).

the sky lines, and second-order corrections are made to the NOT+ALFOSC+Grism4 spectra (Stanishev 2007). The final step in spectral reductions with the QUBA pipeline is the removal of telluric lines, using the standard stars observed in the same night. The fluxes of the reduced spectra were compared with photometry of the SN at the same epoch and, when necessary, multiplied by a constant to correct for slit losses.

The NaCo images were reduced in the standard manner using the XDIMSUM package within IRAF. The sky was subtracted using sky frames created from median-combined dithered on-source images.

The *HST* images (*F*569*W* and *F*814*W* filters acquired on 1995 October 16) were obtained from the ESO archive, and reduced with the On-The-Fly (OFT) pipeline, which applies the most up-to-date calibrations available at the time of request. Multiple exposures were taken in each filter to facilitate the rejection of cosmic rays. These images were combined using the CRREJ task within the IRAF STSDAS package. The site of the SN fell upon the WF4 chip, which has a pixel scale of 0.1 arcsec pixel^{-1}.

APPENDIX B: TOY MODEL AND Ib SNe

Valenti et al. (2008a) introduced a toy model to compute a first-order estimate of the main physical parameters M_{56Ni}, M_{ej} and E_k. Here, we report the application of this toy model to five well-studied He-rich SNe (2008D, 1999dn, 2008ax, 2007Y and 2009jf) and discuss some caveats.

The photospheric velocities at maximum (used as scale velocity; see Arnett 1982) are reported in Table B1, together with the values obtained from the model fit and values from the literature. The nickel masses obtained with our toy model are consistent with the values from more elaborate models. The ejecta masses for SNe 2008ax and 2008D are also in agreement with other estimates. On the other hand, the kinetic energies obtained for SNe 2008D and 2008ax are larger than those obtained by detailed models.

We stress that there are caveats inherent in this toy model. The model uses a constant opacity (we used $k_{opt} = 0.06$ as in Valenti et al. 2008a), while in reality the opacity changes as the SN expands. Using a larger value for the optical opacity results in a lower ejected mass and kinetic energy (see also Chatzopoulos et al. 2009). The model also uses a single velocity (*scale velocity*) that to first order can be approximated as the photospheric velocity at maximum (Arnett 1982). Since no density structure is considered, the toy model will not distinguish among objects with similar photospheric velocities and light curves, but different density profiles. The last important caveat concerns the time interval during which the optically thick (photospheric) and optically thin (nebular) approximations are valid. For slowly evolving SNe (e.g. SN 2009jf), the ejecta can be safely considered optically thick until 40 d after *B*-band maximum, while for the fast evolving SNe 1994I or 2007Y, the SN is no longer completely optically thick ∼20 d after maximum. We also note that the model fit is poor soon after explosion, probably because the point-source approximation[25] is not valid at this time. Thus we usually fit the model bolometric curve (in the photospheric phase) from 15–10 d before maximum to 20–40 d after maximum (depending on the speed of evolution of the SN, as shown in Fig. B1).

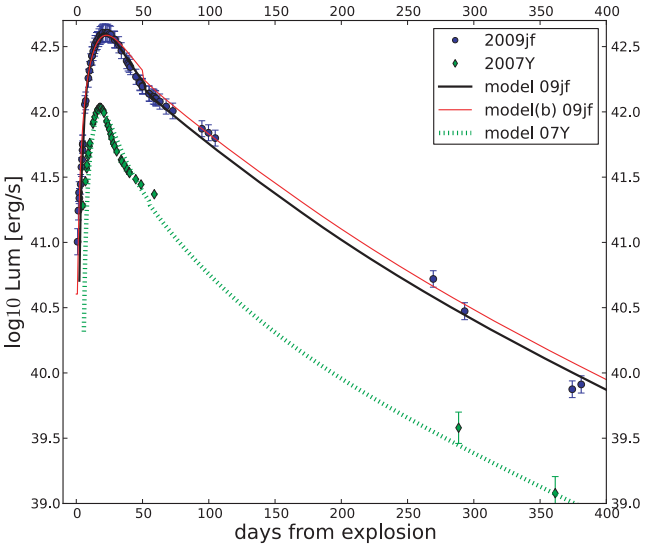

Figure B1. The bolometric light curves of SNe 2009jf and 2007Y and the toy models that fit the light curves. The toy model labelled with (b) was obtained using also the points soon after the explosion. This model cannot reproduce nicely the peak, overestimating the ejected mass and kinetic energy.

[25] All the nickel concentrated in one point at the centre of the SN.

APPENDIX C: TABLES

Table C1. Optical photometry of SN 2009jf reference stars (Vega magnitudes in Landolt system).[a]

ID	*U*	*B*	*V*	*R*	*I*
1	–	16.054 (014)	15.275 (003)	14.844 (002)	14.427 (014)
2	17.052 (06)	16.717 (026)	15.881 (014)	15.406 (039)	14.947 (011)
3	–	16.712 (024)	16.029 (023)	15.602 (017)	15.209 (023)
4	–	15.930 (030)	15.139 (013)	14.726 (016)	14.332 (020)
5	18.805 (13)	18.062 (043)	17.048 (020)	16.420 (013)	15.894 (023)
6	17.890 (15)	17.654 (017)	16.812 (012)	16.280 (014)	15.802 (018)
7	17.186 (10)	17.196 (012)	16.509 (022)	16.124 (017)	15.701 (014)
8	–	18.664 (030)	17.088 (062)	16.468 (051)	15.801 (020)
9	–	15.854 (030)	14.848 (020)	14.340 (003)	13.841 (004)
10	–	14.736 (019)	14.053 (011)	13.648 (020)	13.235 (020)
11	–	18.618 (034)	17.345 (044)	16.460 (006)	15.600 (020)
12	–	15.376 (020)	14.620 (020)	14.245 (020)	13.820 (020)
13	19.051 (23)	18.022 (038)	16.973 (049)	16.352 (020)	15.821 (028)
14	18.577 (16)	17.385 (029)	16.185 (015)	15.424 (024)	14.826 (008)
15	–	16.715 (030)	15.441 (012)	14.750 (020)	14.163 (020)
16	–	18.419 (050)	16.881 (031)	16.097 (016)	15.309 (018)
17	15.966 (07)	15.371 (011)	14.457 (009)	13.947 (021)	13.530 (025)
19	14.556 (02)	14.303 (011)	13.421 (019)	12.926 (012)	12.425 (010)
20	17.755 (06)	16.991 (029)	15.945 (020)	15.285 (018)	14.699 (017)

[a]The uncertainties are the standard deviation of the mean of the selected measurements.

Table C2. Optical photometry of SN 2009jf reference stars (AB magnitudes in Sloan system).[a]

ID	*u*	*g*	*r*	*i*	*z*
2	17.880 (065)	16.286 (023)	15.634 (027)	15.399 (019)	15.300 (011)
5	19.473 (105)	17.591 (028)	16.688 (027)	16.360 (022)	16.210 (031)
6	18.781 (047)	17.247 (029)	16.539 (018)	16.251 (014)	16.150 (040)
7	18.072 (055)	16.871 (031)	16.337 (017)	16.129 (023)	16.069 (034)
13	–	17.544 (039)	16.614 (023)	16.274 (024)	16.053 (026)
14	–	16.795 (014)	15.711 (040)	15.303 (016)	15.092 (032)
17	16.680 (038)	14.917 (029)	14.189 (023)	13.975 (022)	13.906 (025)
18	–	–	18.033 (058)	16.560 (055)	15.849 (029)
19	15.408 (023)	13.834 (010)	13.154 (015)	12.863 (020)	12.727 (020)
20	18.596 (055)	16.472 (026)	15.563 (021)	15.181 (022)	14.981 (022)

[a]The uncertainties are the standard deviation of the mean of the selected measurements.

Table C3. Optical photometry of SN 2009jf (Vega magnitudes in Landolt system).[a]

Date	JD (−240 0000)	Phase[b]	*U*	*B*	*V*	*R*	*I*	Source[c]
2009-09-23	55097.51	−21.9	–	>19.5	>19.0	>18.5	–	NAR
2009-09-24	55098.51	−20.0	–	>19.5	>19.0	>18.6	–	NAR
2009-09-26	55100.50	−18.9	–	19.12 0.50	18.90 0.56	18.42 0.32	–	NAR
2009-09-26	55101.11	−18.3	–	–	–	17.91	–	IAUC
2009-09-27	55101.61	−17.8	–	18.30 0.600	17.92 0.39	17.63 0.23	–	NAR
2009-09-29	55103.58	−15.8	–	–	17.36 0.20	–	–	RCOS20
2009-09-30	55104.58	−14.8	–	–	17.00 0.10	–	–	RCOS20
2009-10-01	55105.60	−13.8	–	–	16.55 0.10	–	–	RCOS20
2009-10-01	55106.00	−13.4	–	–	16.376 0.073	16.136 0.079	16.030 0.077	PROMPT
2009-10-02	55106.63	−12.8	16.910 0.028	16.917 0.012	16.359 0.010	16.138 0.007	16.016 0.011	TNG
2009-10-02	55106.64	−12.8	–	16.927 0.041	–	–	–	PROMPT
2009-10-04	55108.62	−10.8	–	–	–	15.693 0.010	–	FORS2
2009-10-04	55109.41	−10.0	16.200 0.202	16.310 0.015	15.805 0.011	15.550 0.014	15.424 0.013	LT
2009-10-05	55109.61	−9.8	–	–	15.65 0.10	–	–	RCOS20
2009-10-05	55110.33	−9.1	–	15.97 0.12	15.66 0.15	15.45 0.18	15.32 0.11	AN1
2009-10-06	55111.36	−8.0	15.864 0.012	15.888 0.017	15.538 0.016	15.267 0.018	15.268 0.031	CA

Table C3 – *continued*

Date	JD (−240 0000)	Phase[b]	*U*	*B*	*V*	*R*	*I*	Source[c]
2009-10-06	55111.38	−8.0	15.870 0.029	15.947 0.009	15.510 0.009	15.333 0.018	15.214 0.011	LT
2009-10-07	55112.31	−7.1	–	15.90 0.15	15.36 0.12	15.17 0.16	15.13 0.16	AN1
2009-10-08	55112.57	−6.8	–	15.848 0.017	–	–	–	PROMPT
2009-10-08	55113.39	−6.0	15.800 0.018	15.791 0.010	15.308 0.007	15.155 0.009	14.988 0.009	LT
2009-10-09	55113.56	−5.8	–	15.724 0.015	15.292 0.015	15.170 0.014	14.958 0.018	PROMPT
2009-10-10	55114.64	−4.8	–	–	–	14.98 0.10	14.90 0.11	PROMPT
2009-10-10	55115.39	−4.0	15.749 0.021	15.681 0.007	15.196 0.007	15.015 0.010	14.879 0.008	LT
2009-10-12	55116.55	−2.8	–	15.592 0.015	15.143 0.011	14.965 0.010	14.803 0.009	PROMPT
2009-10-12	55117.40	−2.0	15.699 0.018	15.570 0.018	15.111 0.008	14.920 0.007	14.737 0.007	LT
2009-10-13	55117.63	−1.8	–	15.602 0.027	15.103 0.044	14.942 0.053	14.707 0.055	PROMPT
2009-10-13	55118.48	−0.9	15.670 0.058	15.584 0.017	15.056 0.015	14.928 0.020	14.665 0.035	NOT
2009-10-14	55119.34	−0.1	15.698 0.022	15.577 0.010	15.046 0.009	14.882 0.010	14.664 0.009	LT
2009-10-15	55119.60	0.2	–	15.600 0.061	15.010 0.018	14.859 0.015	14.648 0.013	PROMPT
2009-10-16	55121.45	2.1	15.740 0.040	15.581 0.017	15.045 0.013	14.861 0.013	14.639 0.014	A1.82
2009-10-18	55122.53	3.1	–	15.620 0.029	15.034 0.010	14.850 0.011	14.584 0.013	PROMPT
2009-10-18	55123.37	4.0	15.858 0.040	15.623 0.019	15.046 0.015	14.812 0.005	14.563 0.006	A1.82
2009-10-20	55124.62	5.2	16.046 0.007	15.698 0.018	15.061 0.012	14.838 0.011	14.560 0.008	NTT
2009-10-21	55125.52	6.1	–	15.771 0.015	15.034 0.027	14.885 0.023	14.615 0.020	PROMPT
2009-10-23	55128.34	8.9	16.468 0.015	15.937 0.015	15.157 0.016	14.851 0.017	14.614 0.016	LT
2009-10-24	55128.57	9.2	–	15.945 0.020	15.163 0.014	14.856 0.010	14.657 0.010	PROMPT
2009-10-25	55129.54	10.1	–	16.022 0.017	–	–	–	PROMPT
2009-10-27	55131.54	12.1	–	16.171 0.022	15.271 0.012	14.950 0.008	14.673 0.011	PROMPT
2009-10-27	55132.60	13.2	–	–	15.381 0.086	–	–	FORS2
2009-10-29	55133.52	14.1	–	16.440 0.039	15.447 0.015	14.999 0.037	14.759 0.052	PROMPT
2009-11-02	55137.52	18.1	–	16.860 0.031	15.697 0.017	15.199 0.016	14.866 0.016	PROMPT
2009-11-03	55138.54	19.1	–	16.929 0.045	15.726 0.089	15.258 0.019	14.924 0.013	PROMPT
2009-11-03	55139.33	19.9	17.632 0.103	16.937 0.012	15.797 0.010	15.235 0.008	14.906 0.010	LT
2009-11-04	55140.38	21.0	17.600 0.035	17.043 0.014	15.874 0.018	15.322 0.029	14.969 0.019	NOT
2009-11-06	55141.52	22.1	–	17.081 0.040	–	–	–	PROMPT
2009-11-09	55144.56	25.2	–	–	–	15.548 0.023	15.120 0.024	PROMPT
2009-11-11	55147.33	27.9	17.969 0.045	17.381 0.014	16.215 0.008	15.586 0.009	15.258 0.011	LT
2009-11-12	55147.54	28.1	–	17.427 0.045	16.220 0.021	15.666 0.017	15.247 0.014	PROMPT
2009-11-12	55147.54	28.1	–	–	16.235 0.018	–	–	PROMPT
2009-11-13	55149.34	29.9	18.070 0.070	17.440 0.014	16.274 0.009	15.652 0.007	15.340 0.009	LT
2009-11-13	55149.37	30.0	18.050 0.041	17.437 0.014	16.286 0.009	15.780 0.012	15.330 0.013	NOT
2009-11-14	55149.53	30.1	–	–	16.305 0.029	15.728 0.018	15.303 0.015	PROMPT
2009-11-18	55154.41	35.0	18.080 0.192	17.584 0.017	16.482 0.015	15.906 0.012	15.397 0.029	CA
2009-11-19	55154.54	35.1	–	17.605 0.054	16.502 0.049	15.936 0.066	15.433 0.056	PROMPT
2009-11-22	55157.52	38.1	18.249 0.101	17.683 0.032	16.558 0.029	15.980 0.006	15.511 0.017	NTT
2009-11-23	55158.26	38.9	18.141 0.003	17.702 0.015	16.568 0.014	16.000 0.013	15.508 0.012	CA
2009-11-23	55159.35	39.9	18.250 0.104	17.718 0.048	16.564 0.050	15.982 0.012	15.594 0.010	LT
2009-11-24	55159.56	40.2	–	17.721 0.25	16.62 0.20	16.014 0.017	15.576 0.016	PROMPT
2009-11-27	55162.53	43.1	–	17.800 0.077	16.680 0.057	16.047 0.018	15.633 0.015	PROMPT
2009-12-01	55167.32	47.9	18.333 0.098	17.830 0.055	16.751 0.059	16.146 0.012	15.793 0.012	LT
2009-12-06	55172.34	52.9	18.336 0.068	17.84 0.11	16.80 0.11	16.277 0.009	15.869 0.008	LT
2009-12-28	55194.30	74.9	–	–	–	16.664 0.075	16.196 0.065	CA
2009-12-29	55195.29	75.9	18.456 0.172	18.09 0.20	17.14 0.19	–	16.214 0.045	CA
2010-01-02	55199.27	79.9	>17.97	–	17.229 0.058	16.746 0.061	16.273 0.060	CA
2010-01-07	55204.36	85.0	18.464 0.067	18.143 0.012	17.324 0.010	16.869 0.016	16.412 0.015	NOT
2010-06-18	55368.90	249.5	–	20.483 0.088	20.164 0.081	19.368 0.042	19.273 0.051	NTT
2010-07-14	55392.57	273.2	–	21.44 0.57	20.68 0.42	19.81 0.16	19.97 0.15	CA
2010-10-04	55473.78	354.4	–	–	22.00 0.20	21.39 0.16	–	NTT
2010-10-11	55480.54	361.1	–	–	–	21.30 0.43	–	FORS2

[a]The errors are computed taking into account both the uncertainty of the PSF fitting of the SN magnitude and the uncertainty due to the background contamination (computed by an artificial-star experiment).

[b]Relative to the *B*-band maximum (JD = 245 5119.4).

[c]IAUC = IAU Circular 8232. A1.82 = Asiago 1.82-m telescope and AFOSC; pixel scale = 0.473 arcsec pixel^{-1}. NOT = Nordic Optical Telescope and ALFOSC; pixel scale = 0.188 arcsec pixel^{-1}. TNG = Telescopio Nazionale Galileo and DOLORES; pixel scale = 0.25 arcsec pixel^{-1}. PROMPT = PROMPT telescopes and CCD camera Alta U47UV E2V CCD47−10; pixel scale = 0.590 arcsec pixel^{-1}. FORS2 = 8.2-m ESO-VLT Telescope and FORS2, pixel scale = 0.124 arcsec pixel^{-1}. CA = Calar Alto 2.2-m Telescope + CAFOS; pixel scale = 0.53 arcsec pixel^{-1}. LT = Liverpool Telescope and RATCam; pixel scale = 0.279 arcsec pixel^{-1}. NTT = New Technology telescope and EFOSC2; pixel scale = 0.24 arcsec pixel^{-1}. NAR = Newtonian Astrograph Reflector and Canon EOS 350D camera. AN1 = AlbaNova 1-m telescope and DV438. RCOS20 = 20 arcsec RCOS and STL11K; pixel scale = 0.9 arcsec pixel^{-1}.

Table C4. Optical photometry of SN 2009jf (AB magnitudes in Sloan system).[a]

Date	JD (−240 0000)	Phase[b]	*u*	*g*	*r*	*i*	*z*	Source[c]
2009-10-04	55109.41	−10.0	–	–	15.767 0.013	15.808 0.013	–	LT
2009-10-06	55111.38	−8.0	–	–	15.518 0.008	15.572 0.011	–	LT
2009-10-08	55113.39	−6.0	16.688 0.018	15.569 0.008	15.343 0.009	15.388 0.009	15.438 0.016	LT
2009-10-08	55113.55	−5.8	–	15.428 0.092	15.304 0.036	15.309 0.040	15.334 0.077	PROMPT
2009-10-10	55115.39	−4.0	16.644 0.022	15.394 0.017	15.208 0.010	15.261 0.008	15.240 0.016	LT
2009-10-12	55116.56	−2.8	–	15.390 0.015	15.114 0.015	15.185 0.015	15.207 0.017	PROMPT
2009-10-12	55117.41	−2.0	16.552 0.024	15.327 0.015	15.098 0.009	15.138 0.010	15.169 0.017	LT
2009-10-13	55117.62	−1.8	–	15.350 0.024	15.129 0.028	15.150 0.019	15.090 0.028	PROMPT
2009-10-14	55119.35	−0.1	16.568 0.024	15.328 0.018	15.040 0.010	15.056 0.009	15.080 0.012	LT
2009-10-15	55119.62	0.2	–	15.305 0.024	15.009 0.011	15.005 0.019	15.045 0.021	PROMPT
2009-10-18	55122.53	3.1	–	–	14.963 0.013	15.002 0.016	14.942 0.024	PROMPT
2009-10-21	55125.53	6.1	–	15.429 0.012	14.944 0.018	14.987 0.016	14.929 0.023	PROMPT
2009-10-23	55128.34	8.9	17.301 0.021	15.527 0.015	15.020 0.017	15.010 0.016	14.978 0.010	LT
2009-10-24	55128.51	9.1	–	15.557 0.011	–	–	–	PROMPT
2009-10-25	55129.55	10.1	–	15.575 0.011	–	–	–	PROMPT
2009-10-27	55131.52	12.1	–	15.711 0.010	15.112 0.012	15.064 0.010	15.030 0.014	PROMPT
2009-10-28	55132.53	13.1	–	15.777 0.016	15.178 0.036	15.125 0.016	15.065 0.014	PROMPT
2009-11-03	55138.54	19.1	–	16.314 0.061	15.456 0.016	15.353 0.010	15.244 0.037	PROMPT
2009-11-03	55139.34	19.9	18.370 0.039	16.408 0.008	15.499 0.010	15.336 0.010	15.263 0.016	LT
2009-11-05	55140.52	21.1	–	16.400 0.012	–	15.441 0.012	15.288 0.030	PROMPT
2009-11-11	55147.33	27.9	–	–	15.869 0.016	15.710 0.006	15.479 0.024	LT
2009-11-13	55148.78	29.4	–	16.967 0.017	15.969 0.015	15.804 0.006	15.499 0.015	PROMPT
2009-11-13	55149.35	29.9	18.966 0.136	17.004 0.018	15.961 0.015	15.789 0.015	15.531 0.012	LT
2009-11-19	55154.52	35.12	–	–	16.128 0.017	15.990 0.010	15.605 0.008	PROMPT
2009-11-23	55159.36	40.0	19.122 0.039	17.167 0.018	16.241 0.015	16.055 0.009	15.640 0.009	LT
2009-11-24	55159.52	40.1	–	–	16.199 0.017	16.081 0.019	15.647 0.019	PROMPT
2009-12-01	55167.32	47.9	19.151 0.098	17.249 0.026	16.381 0.012	16.240 0.010	15.785 0.013	LT
2009-12-02	55167.55	48.1	–	–	16.396 0.013	16.259 0.016	–	PROMPT
2009-12-06	55172.34	52.3	19.206 0.056	17.283 0.017	16.429 0.013	16.301 0.012	15.892 0.044	LT

[a]The errors are computed taking into account both the uncertainty of the PSF fitting of the SN magnitude and the uncertainty due to the background contamination (computed by an artificial-star experiment).
[b]Relative to the *B*-band maximum (JD = 245 5119.4).
[c]PROMPT = Prompt telescopes and CCD camera Alta U47UV E2V CCD47−10; pixel scale = 0.590 arcsec pixel^{-1}. LT = Liverpool Telescope and RATCam; pixel scale = 0.279 arcsec pixel^{-1}.

Table C5. IR photometry of SN 2009jf.[a]

Date	JD (−240 0000)	Phase[b]	*J*	*H*	*K*	Source[c]
2009-10-02	55106.59	−12.8	15.565 0.029	15.511 0.042	15.356 0.052	NICS
2009-10-07	55111.45	−7.9	14.838 0.016	14.725 0.018	14.527 0.021	NICS
2009-10-13	55117.31	−2.1	14.42 0.11	14.393 0.093	14.29 0.14	NICS
2009-10-20	55125.64	6.2	14.285 0.011	14.151 0.011	13.956 0.015	SOFI
2009-10-23	55128.35	8.9	14.305 0.067	14.335 0.089	–	LT
2009-10-24	55129.39	10.0	14.32 0.13	14.19 0.15	–	LT
2009-10-27	55132.02	12.6	14.36 0.20	14.18 0.20	–	REM
2009-11-06	55141.16	21.8	14.52 0.14	14.40 0.11	14.30 0.11	REM
2009-11-11	55146.08	26.7	14.77 0.38	14.61 0.41	14.637 0.096	REM
2009-11-15	55150.14	30.7	14.81 0.47	14.79 0.44	14.70 0.26	REM
2009-11-19	55154.14	34.7	14.99 0.37	14.89 0.37	>14.322	REM
2009-11-23	55158.52	39.1	15.069 0.020	14.897 0.024	14.924 0.029	SOFI
2009-11-24	55159.05	39.6	15.11 0.25	14.817 0.25	15.34 0.23	REM
2009-12-08	55174.32	54.9	15.600 0.056	15.140 0.052	–	LT
2010-07-02	55378.68	259.3	19.34 0.30	18.57 0.30	19.08 0.30	NICS

[a]The errors are computed taking into account both the uncertainty of the PSF fitting of the SN magnitude and the uncertainty due to the background contamination (computed by an artificial-star experiment).
[b]Relative to the *B*-band maximum (JD = 245 5119.4).
[c]NICS = Telescopio Nazionale Galileo and NICS; pixel scale = 0.25 arcsec pixel^{-1}. LT = Liverpool Telescope and SupIRCam near-IR camera; pixel scale = 0.41 arcsec pixel^{-1}. REM = Rapid Eye Mount 60-cm telescope and REMIR ; pixel scale = 1.2 arcsec pixel^{-1}. SOFI = NTT telescope and SOFI; pixel scale = 0.29 arcsec pixel^{-1}.

Table C6. *Swift* photometry of SN 2009jf.[a]

Date	JD (−240 0000)	Phase[b]	$uvw1$	U	B	V	Source
2009-09-30	55104.68	−14.7	18.03 0.07	18.01 0.19	17.31 0.05	16.80 0.07	*Swift*
2009-10-01	55105.55	−13.8	18.02 0.07	17.63 0.17	17.13 0.05	16.53 0.07	*Swift*
2009-10-04	55108.97	−10.4	17.90 0.06	16.47 0.14	16.28 0.03	15.80 0.05	*Swift*
2009-10-06	55111.31	−8.1	18.04 0.07	16.03 0.09	15.90 0.03	15.47 0.04	*Swift*
2009-10-08	55113.26	−6.1	18.02 0.08	15.88 0.06	15.77 0.03	15.35 0.04	*Swift*
2009-10-10	55115.14	−4.3	17.85 0.07	15.74 0.06	15.67 0.03	15.22 0.04	*Swift*
2009-10-12	55117.21	−2.2	18.02 0.08	15.76 0.08	15.60 0.04	15.09 0.04	*Swift*
2009-10-14	55119.15	−0.2	18.00 0.06	15.73 0.05	15.60 0.04	15.03 0.04	*Swift*
2009-10-16	55120.54	1.1	17.97 0.07	15.82 0.10	15.62 0.03	15.03 0.04	*Swift*
2009-10-18	55122.82	3.4	17.92 0.06	15.98 0.08	15.62 0.03	15.06 0.04	*Swift*
2009-10-20	55124.55	5.1	18.10 0.07	16.09 0.07	15.73 0.03	15.07 0.04	*Swift*
2009-11-01	55137.14	17.7	18.04 0.07	17.32 0.07	16.75 0.04	15.65 0.04	*Swift*
2009-11-04	55139.56	20.2	18.02 0.08	17.68 0.08	16.915 0.04	15.80 0.05	*Swift*
2009-11-07	55142.64	23.2	–	17.72 0.13	17.21 0.06	–	*Swift*

[a]The U-band data have been reduced using the template-subtraction technique within the QUBA pipeline. The S-correction has been applied. The errors have been computed taking into account both the uncertainty of the PSF fitting of the SN magnitude and the uncertainty due to the background contamination (computed by an artificial-star experiment). The $uvw1$, B and V bands have been reduced using the *Swift* pipeline. The $uvm2$ and $uvw2$ bands have been measured with the *Swift* pipeline but are not reported as they are strongly contaminated by the nearby cluster.

[b]Relative to the B-band maximum (JD = 245 5119.4).

This paper has been typeset from a TEX/LATEX file prepared by the author.